Zigah, Michael P.

ELEVATED PYROGENIC ORGANIC MATTER IN SEDIMENTS FROM LAKE BOSUMTWI, GHANA AS A PROXY FOR THE TERMINATION OF THE AFRICAN HUMID PERIOD

(Under the direction of Dr. Siddhartha Mitra) East Carolina University, Department of Geological Sciences, July 2025

This study investigates the Holocene paleoclimatic history of northern Africa, using total organic carbon (TOC), soot carbon (C_{soot}), and other markers of pyrolysis in a sediment core from Lake Bosumtwi, Ghana, west Africa. The African climate has been dynamic throughout the Quaternary, influenced by multiple drivers varying in duration and magnitude. One particularly notable period is the transition from the African Humid Period (AHP) (~14 - ~5 ka) to the current arid conditions in northern Africa. Sedimentary records from large African lakes can provide insights into climate-driven landscape changes caused by droughts, wildfires, flooding, and erosion.

A key proxy for wildfires is black carbon (BC), formed from the incomplete combustion of organic matter. BC occurs across a size continuum from large charcoal macro-particles which remain near the fire source to smaller sub-micron-sized soot aerosols capable of long-range atmospheric transport. This study hypothesizes that variations in soot concentrations and anhydride sugars from pyrolysis of cellulose served as a proxy for drought and wildfire activity during the AHP termination (~7.4 -~5 ka). Core samples were analyzed using stratigraphic and geochemical techniques, with C_{soot} isolated through demineralization and chemo-thermal oxidation. The findings of this project show a relative increase in the abundance of pyrogenic organic matter and suggests increased wildfires in northern Africa before the end of the AHP. The proportion of soot to charcoal in Lake Bosumtwi sediments suggests increased distal

wildfire activity and aeolian transport of soot before the end of the AHP (7.4 – 5 ka). The isotopic range of the soot carbon shows a distinct change in vegetation around 5 ka and 3 ka. These findings do not support our initial hypothesis that suggested there would be an increase in the combustion of C_3 vegetation around the termination of the AHP, followed by an increase in the combustion of C_4 vegetation. Nonetheless, these results contribute to the understanding of aeolian transport of charred biomass between northern and western Africa, providing constraints on the timing and spatial variability of the AHP termination.

ELEVATED PYROGENIC ORGANIC MATTER IN SEDIMENTS FROM AN AFRICAN LAKE AS A PROXY FOR THE TERMINATION OF THE AFRICAN HUMID PERIOD

A Thesis

Presented to the Faculty of the Department of

Geological Sciences

East Carolina University

In Partial Fulfillment of the Requirements for the Degree of

Master of Science in Geology

By

Michael P. Zigah

July 2025

Director of Thesis: Siddhartha Mitra, P.h.D

Thesis Committee Members;

Meg Blome, P.h.D

David Mallinson, P.h.D

Rosana Ferreira, P.h.D

Dedication

I would like to dedicate this thesis to my wife Chloe, my family, and my cats. I would like to make a special dedication to my cat Frank who is no longer with us. They have all supported me through moments of stress and confusion in my academic career. Thank you all so much.

Acknowledgments

I would like to thank my advisor and major professor, Dr. Siddhartha Mitra, for his assistance and guidance throughout this thesis project. I would also like to thank my committee members, Dr. David Mallinson & Dr. Meg Blome, Department of Geological Sciences, and Dr. Rosana Ferreira, Department of Geography, Planning, and Environment. I would like to give a special thanks to Rachel Wheatley, fellow graduate student and lab mate. All these people provided support in various ways throughout this research project.

I would also like to thank Kristina Brady, director of core repository manager, and others at the University of Minnesota for providing the sediment core and additional invaluable information for this research project.

Finally, I would like to acknowledge Dr. Jason Curtis, Manager, Light Stable Isotope Mass Spectrometer Laboratory, Department of Geological Sciences, University of Florida for his assistance in this thesis project.

Table of Contents

List of Tables

List of Figures

ELEVATED PYROGENIC ORGANIC MATTER IN SEDIMENTS FROM AN AFRICAN LAKE AS A PROXY FOR THE TERMINATION OF THE AFRICAN HUMID PERIOD

I. Introduction

Oceanic and atmospheric systems are integral in distributing and circulating thermal energy from solar radiation. Natural perturbations such as ice rafting events, volcanism, and orbital changes can disrupt oceanic and atmospheric circulation, temporally and spatially affecting regional and global climate (Mayewski et al., 2004; Peck et al., 2004). Several additional factors affect climate change, including emissions of greenhouse gases, albedo, changes in insolation, and orbital cycles like the eccentricity, precession, and obliquity of Earth (Prell et al., 1992; Tuenter et al., 2003; Mayewski et al., 2004; Niedermeyer et al., 2010). These changes affect regional and global climate conditions on time scales from 10^1 to 10^5 years. The impacts of climate can manifest themselves over great distances because of teleconnections between the Earth's ocean and atmosphere (Mayewski et al., 2004; Moore et al., 2022).

The Holocene epoch (11.7 ka-present) is a period of post-glacial warming punctuated by intervals of rapid climate change, like the Eemian interglacial period (ca 130 ka to 115 ka). Both periods had lasting effects on the landscape of northern Africa (Pausata et al., 2020). In Africa, rapid climate change driven by regional atmospheric and ocean circulation systems has had regional and global consequences for precipitation patterns, vegetation coverage, and hominid migration (Maley et al., 1991; Mayewski et al., 2004; McGee et al., 2017; Kuper et al., 2006). For example, the consequences of a modern changing climate caused flooding in Sudan in the 1980's (Sutcliffe et al., 2009) and extensive droughts in northern Mali in the 1990's (Pedersen et al., 1995). Drastic vegetative and hydrological changes in the landscape have been evident in northern Africa's Sahel and Sahara regions in the Late Pleistocene and throughout the Holocene (deMenocal et al., 2000).

Northern Africa is particularly sensitive to drought, making it an ideal region to study rapid climate change. Though it is presently a desert, northern Africa experienced extreme precipitation in the late Quaternary, during the African Humid Period (AHP) (Renssen et al., 2003; McGee et al., 2017; Pausata et al., 2020). During the AHP (~15 ka to 5.4 ka), the Inter-Tropical Convergence Zone (ITCZ), which is a low-pressure airmass that encircles the equator, was further north than its present-day position (Haug et al., 2001).

Specifically, the summer ITCZ was further north than at present during the AHP, resulting in more summer precipitation in northern Africa than today. This increased precipitation supported dense vegetation in the Sahel region between the late Quaternary and middle Holocene (Shanahan et al., 2006, 2012; Hopker et al., 2019,). The strength and extent of ITCZ's migration (Fig. 4) outside of the instrumental records can be reconstructed globally using climate proxies (Sha et al., 2019; Renssen et al., 2003). The termination of the AHP across Africa is considered both temporally and spatially heterogeneous. The southward migration of the ITCZ at the end of the AHP can be explained by the waning of the precession cycle. However, there are many uncertainties tied to the magnitude and extent of the termination of the AHP within northern Africa (DeMenocal et al., 2000).

In northern Africa, the termination of the AHP around 5 ka led to desertification, which coincided with the depopulation of north Africa's interior, including a large exodus of the resident population towards the Nile River ~5 ka (Kuper et al., 2006). This migration played an influential role since early Egypt (~6 ka-5 ka) made significant contributions in the development of modern society, religion, and even agriculture. (Kuper et al., 2006; Midant-Reynes, & Beatrix et al., 2014)

The magnitude and extent of the termination of the AHP remain contentious topics due to a lack of high-resolution paleo archives from the interior of northern Africa. An understanding of the termination of the AHP may shed light on regional drought and population migration as noted in other regions globally (Kuper et al., 2006; McGee et al., 2017).

Despite the multiple lines of evidence of the onset of the AHP around 14 ka, several questions remain regarding the climatic triggers for its termination. Understanding the climatic triggers of termination of the AHP would shed light on the complex interaction between atmospheric circulation and terrestrial vegetation in northern Africa. The termination of the AHP led to droughts and wildfires in northern Africa as it transitioned from humid and vegetated to its present-day hyper-arid state.

Wildfires are commonly associated with periods of drought due to the availability of dry combustible biomass. The burning of vegetation creates pyrolyzed organic matter, which includes solid residues such as charcoal, soot, and other forms of black carbon (BC) and polycyclic aromatic hydrocarbons, levoglucosan (and isomers) (Kuo et al., 2008; Louchouarn et al., 2008, Mitra et al., 2009). Pyrogenic carbon exists along a combustion continuum (Fig. 1). Characteristics of pyrogenic residue in sediments have been used to deconvolve the source of the burned material and provide information on the temperature associated with the fire (Mitra et al., 2009; Thevenon et al., 2010; Tan et al., 2023). For example, in the sedimentary record, the presence of levoglucosan isomers (mannosan and galactosan), anhydrous sugars or fire sugars, suggests that fire temperatures did not exceed ~350 °C (Kuo et al., 2008, Tan et al., 2023). Moreover, the relative abundance of larger charcoal compared to smaller particles like soot and levoglucosan in the sedimentary record may be indicative of a regional wildfire (Thevenon et al., 2010). Wildfire frequency and intensity should coincide with periods of droughts and the presence of various pools of pyrogenic organic matter in sediments can serve as a proxy for periods of drought. In that context, up-core trends in pyrogenic organic matter isolated from lake sediments in northern Africa may contain a proxy record of the transition of the AHP to its present state of aridity.

	Slightly charred biomass	Char	Charcoal	Spheroidal carbonaceous particles (SCP)	Soot
Formation T	low	→			high
Size	mm and larger		mm to µm	µm	nm
Composition and formation	residue of burnt material (biomass and coals)			residue of fossil fuel combustion	combustion condensate
Plant or fuel structures	abundant	significant presence	few	few	none
Reactivity	high	→			low
Drift range	short (m)	short (m to km)		intermediate (km to 1000s of km)	long (up to several 1000s of km)

Figure 1. Combustion continuum with lower temperature conditions and residue on the left and higher temperature residue on the right. Organic molecules such as levoglucosan and PAHs are created by the pyrolysis process all along the continuum (Masiello et al., 2004).

II. Research Questions and Hypotheses

Up-core trends in pyrogenic organic matter isolated from lake sediments in western Africa may reflect the transition of the Sahara during the AHP to its present state of hyperaridity, highlighting the consequences of the loss of vegetative biomass as a function of decreased precipitation. Lake Bosumtwi is an ideal study site due to its position (Fig. 2A) relative to the ITCZ migration path. During the winter months in northern Africa, dry, dusty air is blown from the Sahara across west Africa via the northeasterly Trade winds (prevailing winds associated with ITCZ migration). This seasonal phenomenon serves as the transport mechanism for the deposition of pyrogenic organic matter from northern Africa towards Lake Bosumtwi, evident by paleoclimate proxies for changes related to the ITCZ positioning (Fig. 4) such as dust flux and precipitation (Moore et al., 2022; Niedermeyer et al., 2010). Sediments from Lake Bosumtwi in Ghana, west Africa, were used to address the research question and hypotheses outlined below.

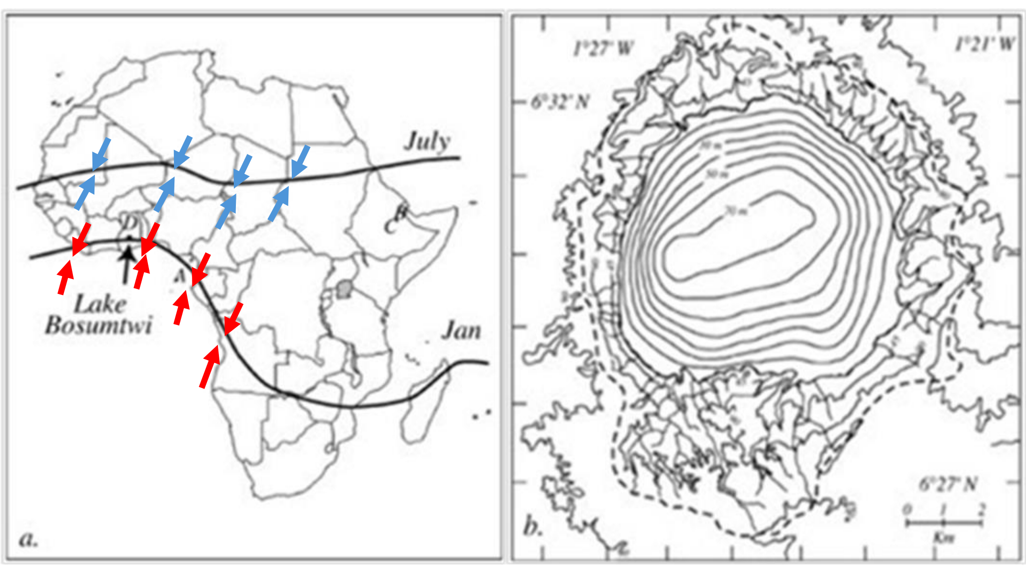

Figures 2a) the seasonal wandering of ITCZ over Africa (blue vectors show northeasterly wind direction in summer months, red vectors show the direction during winter months) and 2b) the bathymetry of crater lake Bosumtwi and cardinal positioning (Otu et al 2010).

The overarching scientific question being addressed is: do pyrogenic markers in the sedimentary record of Lake Bosumtwi (Ghana) serve as proxies for changes in fire regimes that are coincident with the termination of the AHP (~5 ka). The hypotheses below were tested to address this overarching question:

H1: A southward migration of the ITCZ across the African continent may have led to drought conditions through much of northern Africa, eventually leading to the termination of the AHP.

Soot is smaller than charcoal, allowing for its aeolian transport with greater ease than charcoal. Therefore, elevated concentrations of soot relative to charcoal within the same event horizon at the end of the AHP would suggest an increase in distal wildfires brought on by the weakening of monsoons (because of the southward retreat of the summer ITCZ positioning) and increased aridity in northern Africa. If this hypothesis is supported, then the relative abundance of pyrogenic organic matter such as soot, levoglucosan isomers (fire sugars) and charcoal in Lake Bosumtwi's sedimentary record will increase coeval with the collapse of the AHP. In northern Africa (Sahara and Sahel regions) the end of the AHP occurs closer to north 5 ka, while more southern regions like lake Bosumtwi (Ghana) west experience it closer to 3 ka. These termination ages are based on isotope proxies for humidity and changes in dust fluxes across northern Africa (Moore et al., 2022; Niedermeyer et al., 2010).

H2: Evidence of drought conditions in northern Africa before the end of the AHP (7. ka-~5 ka) may be evident in the record of Lake Bosumtwi's sediments (Fig. 2), through the comparison of aeolian soot to charcoal particle counts and abundance of fire sugars in upcore sediments.

During winter months, northeasterly trade winds transport substantial amounts of aeolian sediments from the Sahara in the east, towards west Africa. These Trade Winds serve as the annual aeolian transport mechanism for C_{Soot} and levoglucosan isomer deposition from northern Africa. Thus, if this hypothesis is supported, soot should be present at higher abundances in the lake sediments during the termination of the AHP in northern Africa around 5 ka. The period of distal drought around 5 ka associated with the collapse of the AHP will coincide with higher ratios of soot relative to charcoal in Bosumtwi's sedimentary record of that time. Higher ratios of charcoal to soot will be present in Lake Bosumtwi's sediments at ca. 3 ka when coastal west Africa would experience the end of the AHP.

H3: The $\delta^{13}C$ values of pyrogenic organic matter in sediments delineate the source of combusted biomass.

If this hypothesis is supported, then periods of AHP termination in northern Africa will coincide with an increase in the relative abundance of drought-susceptible C3-derived pyrolyzed soot, followed by an increase of drought-tolerant C4-derived pyrolyzed and non-pyrolyzed organic matter. Thus, the isotopic range of the total organic carbon (TOC) and soot carbon ($\delta^{13}C_{TOC}$ and $\delta^{13}C_{soot}$) will be more depleted before 5 ka and then become more enriched (more positive) following the termination of the AHP in sediments from Lake Bosumtwi after 5 ka.

III. Background

A. ITCZ Migration, Drought, and Societal Impacts

The Intertropical Convergence Zone (ITCZ) plays a crucial role in shaping tropical hydrological cycles. Haug et al. (2001) reconstructed Holocene changes in ITCZ position using titanium (Ti) concentrations in sediment cores from the Cariaco Basin adjacent to northern Venezuela. The Cariaco Basin has well preserved continuous sedimentation due to oxygen-depleted bottom water, allowing for well laminated sediments. Sedimentary records in the Cariaco Basin have been used titanium (Ti) and iron (Fe) abundance as indicators of terrigenous runoff as a proxy for rainfall derived erosion. The Cariaco Basin lies just north of the modern mean summer position of the ITCZ, making it an ideal location for reconstructing the latitudinal shifts of the ITCZ. Haug et al. observed a marked decrease in Ti concentrations beginning around 5,000 years ago, indicating reduced precipitation, and suggesting a gradual southward migration of the mean summer ITCZ position during the late Holocene.

In alignment with the southward migration of the ITCZ documented by Haug et al. (2001), Hodell et al. (1995) provided compelling evidence that prolonged droughts in Mesoamerica contributed to the collapse of the Classic Maya civilization. Their study analyzed oxygen isotope ratios ($\delta^{18}O$) in ostracod shells from sediment cores taken from Lake Chichancanab on the Yucatán Peninsula spanning the last several thousand years. A positive $\delta^{18}O$ excursion, reflecting higher ratios of ^{18}O to ^{16}O, indicates an elevated evaporation-to-precipitation (E/P) ratio, interpreted as prolonged drought conditions. These isotopic shifts were especially pronounced between ~1,200 and 1,000 years ago (ca. AD 800–1000), coinciding with the terminal collapse of the Maya civilization. Hodell et al. (1995) attributed this hydrological change to a weakening of the North American monsoon system, possibly linked to broader tropical climate dynamics, including ITCZ shifts. Their findings underscore the role of persistent climate stress in particular, severe droughts effects in driving social and cultural transformations in Mesoamerica during the late Holocene. Additionally, in the Chesapeake Bay, the Holocene drought associated with the migration of the ITCZ was suggested to be coeval with paleo records of regional droughts (Mitra et al., 2009). Thus, large-scale migrations of the ITCZ can influence regional drought, and these shifts have been suggested to be linked to population migration and societal collapse (Haug et al., 2001; Hodell et al., 1995; Mitra et al., 2009).

Study site and paleo-reconstructions

Many African lakes and drilling sites in the Southeastern Atlantic coastal ocean adjacent to Northern Africa have been the subject of the paleoenvironmental (Talbot et al., 1980, Russell et al., 2003, Shanahan et al., 2004, 2006). Many of the Great Lakes in Africa were formed after divergent tectonic activity in the Great Rift Valley of eastern Africa (Magdi et al., 2023). The unique topography of the region allows for the accumulation of water in deep rifts that form in the tectonically divergent zone. Some deep lakes are the result of meteorite impacts, which were filled over thousands of years. Lake Bosumtwi is an example of a lake formed by a meteorite impact that is 1.07 million years old (Jones et al., 1981; Vinnepand et al., 2024).

B1. Lake Bosumtwi

Lake Bosumtwi is an ideal study site to investigate the cessation of the AHP, due to its location and its excellent preservation of in situ sediments. Lake Bosumtwi is in Ghana, west Africa (6°30′N, 1°25′W) and occupies a ~1.07 Mya meteorite impact crater (Jones et al., 1981; Koeberl et al., 2007; Otu et al., 2010; Vinnepand et al., 2024). Ghana lies along the coast of west Africa with close regional proximity to the Gulf of Guinea. Presently, Lake Bosumtwi is affected by various wind and precipitation regimes as the ITCZ migrates northward in the boreal summer and southward in boreal winter. The location of the lake with respect to the ITCZ's annual migration pattern helps determine patterns of lake sedimentation. In the summer months, the ITCZ is at its most northward position away from the lake (Fig. 2a), and the winds are from the southwest. During the fall months, the ITCZ is situated closer to the northern end of the lake and provides higher rainfall to the region of west Africa. The winter months, known as the Harmattan season, are dominated by dry, dusty northeasterlies from the Sahara and Sahel regions of north Africa (Gasse et al., 2000).

The lake is meromictic and hydrologically closed. Thus, fluxes of water are solely driven by cycles of precipitation and evaporation (Shanahan et al., 2006). The depth of the lake (76 meters) leads to anoxia in the hypolimnion, allowing for the preservation of sediments undisturbed by bioturbation or wind-driven mixing. The large catchment area (106 km^2) and established hypolimnion of the lake's water column allow for the deposition and preservation of aeolian sediments from distant regions (Peck et al., 2004; Vinnepand et al., 2024). Thus, Lake Bosumtwi is an ideal location to study environmental changes associated with climate change during the AHP.

Late Quaternary reconstructions of Lake Bosumtwi's water levels have been carried out by multiple researchers to better understand changes in the hydrological cycle during the Holocene and late Pleistocene (Maley et al., 1991; Russell et al., 2003; Shanahan et al., 2006). The lake level reconstruction curve (Fig. 3A) is based on paleo-shorelines and exposed outcrop stratigraphy. In this figure, dashed blue lines indicate uncertainty ranges, colored markers denote materials used for radiocarbon dating, and grey boxes show the locations of paleo-shorelines.

Figure 3B presents magnetic hysteresis grain size measurements, derived from lake sediment samples (Peck et al., 2004). These data are influenced by several environmental factors, including lake productivity, diagenesis, evaporation, precipitation, sediment influx, and runoff. The MRS (saturation remanent magnetization) to MS (saturation magnetization) ratio is used to infer the magnetic grain size of magnetite (Fe_3O_4), where higher MRS/MS ratios reflect finer, more magnetically stable grains, and lower ratios indicate coarser, less stable grains. These measurements help reconstruct past limnological conditions in the lake. Figure 3C shows downcore $\delta^{13}C$ values of organic matter from Lake Bosumtwi sediments, which provide insight into changes in the dominant photosynthetic pathways over time.

In terms of lake level changes, Figure 3A records a significant lowstand at ~16.3 ka, corresponding with Heinrich Event 1 (~17 ka), when massive iceberg discharges into the Atlantic Ocean disrupted thermohaline circulation and cooled the climate. Lake levels subsequently rose by approximately 60 meters around 15 ka, followed by a decline during the Younger Dryas (12.9–11.7 ka) (Shanahan et al., 2006; Weldeab et al., 2005).

During the peak of the African Humid Period (AHP) around 11 ka, increased precipitation caused Lake Bosumtwi to overflow its crater rim. This highstand is supported by radiocarbon-dated charcoal in terrace sediments and ^{14}C surface exposure dating of bedrock (Shanahan et al., 2006). A notable drop in lake level occurred around 8.6 ka, interpreted as a significant drought event. Lake levels recovered after this and remained relatively high until ~5.4 ka. Around 4 ka, lake levels decreased to near present-day values. Later fluctuations include an increase to 20–25 meters above modern levels around 3.5 ka, followed by a decline to ~19

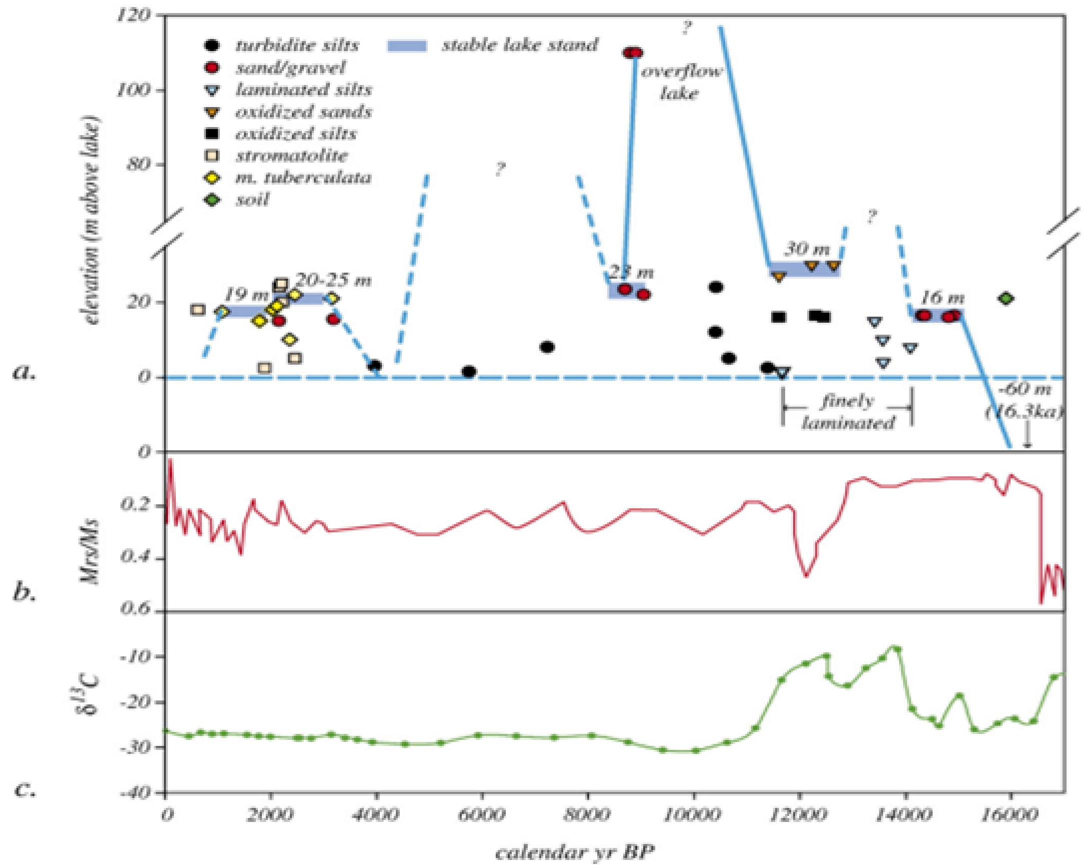

Figure 3. Lake Bosumtwi water level reconstruction using (A) exposed outcrop sediments and paleo shoreline deposits from around the lake, the solid blue shows lake level reconstruction, while the dashed lines represent areas of uncertainty (B) Magnetic hysteresis grain size measurements, and (C) the $\delta^{13}C$ of bulk organic matter of the lake sediments (Shanahan et al 2006).

meters above present levels around 2 ka. Subsequently, the lake depth fell to approximately 70 meters, near its modern depth.

B2. Regional Climate and Seasonality in Ghana

Africa's atmospheric circulation is controlled by multiple air masses, the Intertropical Convergence Zone (ITCZ), its associated trade winds, the westerlies, and the Congo Air Boundary (CAB). The ITCZ is associated with thunderstorms and considerable amounts of precipitation in equatorial regions. The ITCZ is known to seasonally wander to regions of maximum solar exposure, staggering over the Tropic of Cancer in the summer and over the Tropic of Capricorn in the winter as noted earlier in Figure 2A.

The northern hemisphere's westerlies lie between 30°N and 60°N, bringing dry, cold air from high-pressure regions above north Africa. These regions experience a confluence between moist tropical air and dry polar air, resulting in cloud formation and increased precipitation. The position of the westerlies shifts with changes in global temperature (Goyal et al., 2021). Sea Surface Temperature (SST) also plays a significant role in the wandering of both the ITCZ and westerlies (Nicholson et al., 1981; Blome et al., 2012).

Africa is subject to monsoon systems, including the east African monsoon and the west African monsoon. Monsoons are caused by a difference in both pressure and temperature between the ocean and land during the summer and winter months (Krishnamurti, 1987; Prell et al., 1992; Shanahan et al., 2015). Due to the difference in specific heat capacity of land versus water, land both heats up and loses heat more readily than water. Warm land in the summer months creates low-pressure systems that pull moist ocean air landward, causing increased terrestrial precipitation. In the winter months, the process flips, where low-pressure systems are over the ocean (Fig. 4).

Ghana has two main seasons, the dry season (Nov-Mar) and the wet season (Apr-Jun), and two sub-seasons, the little dry season (Jul-Aug), and the little wet season (Sep-Oct) (Maley et al., 1991). The average annual rainfall collected by a meteorological station along the lake between 2004 and 2007 was approximately 1250 mm per year (Otu et al., 2010).

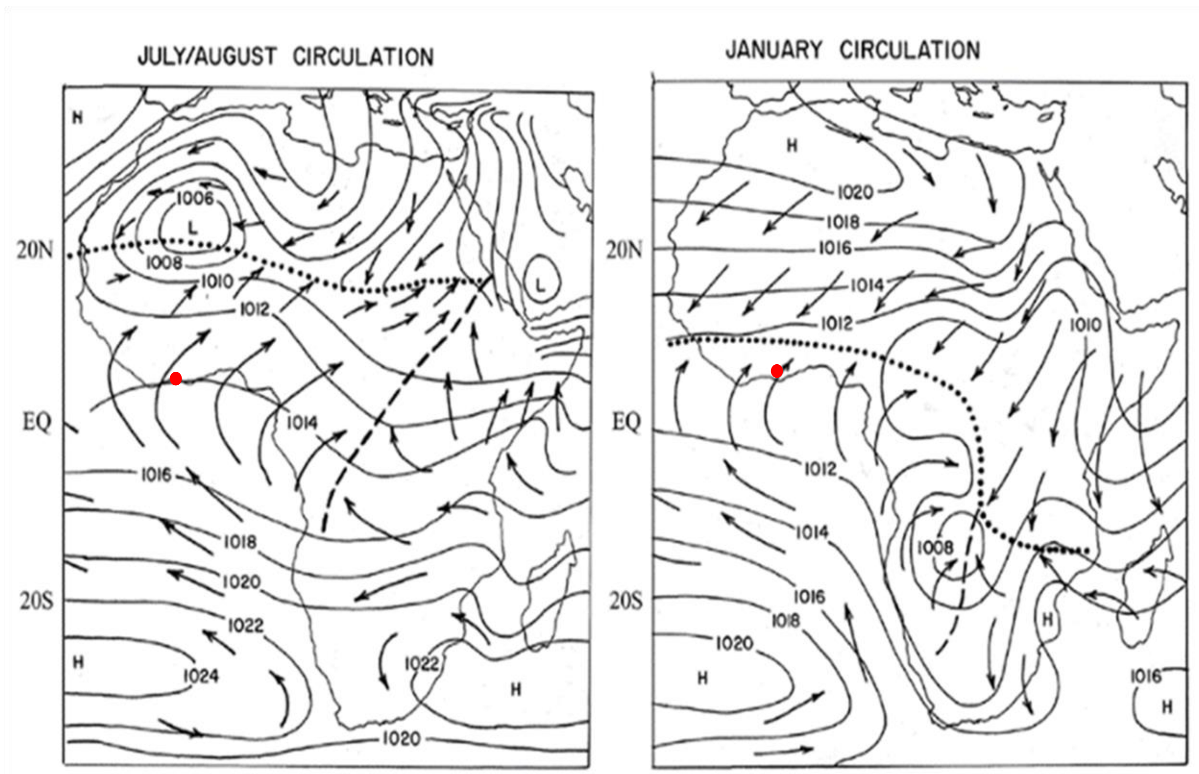

Figure 4 . African summer and winter circulation configuration of the ITCZ (black dotted line) and Congo Air Boundary (CAB) (black dashed lines). The solid black arrows around the ITCZ represent the Tradewinds. The red dot shows the relative positioning of African Lake Bosumtwi (Nicholson et al., 2018).

Most of the rainfall occurs from April through October, with a slight decrease in rainfall in peak

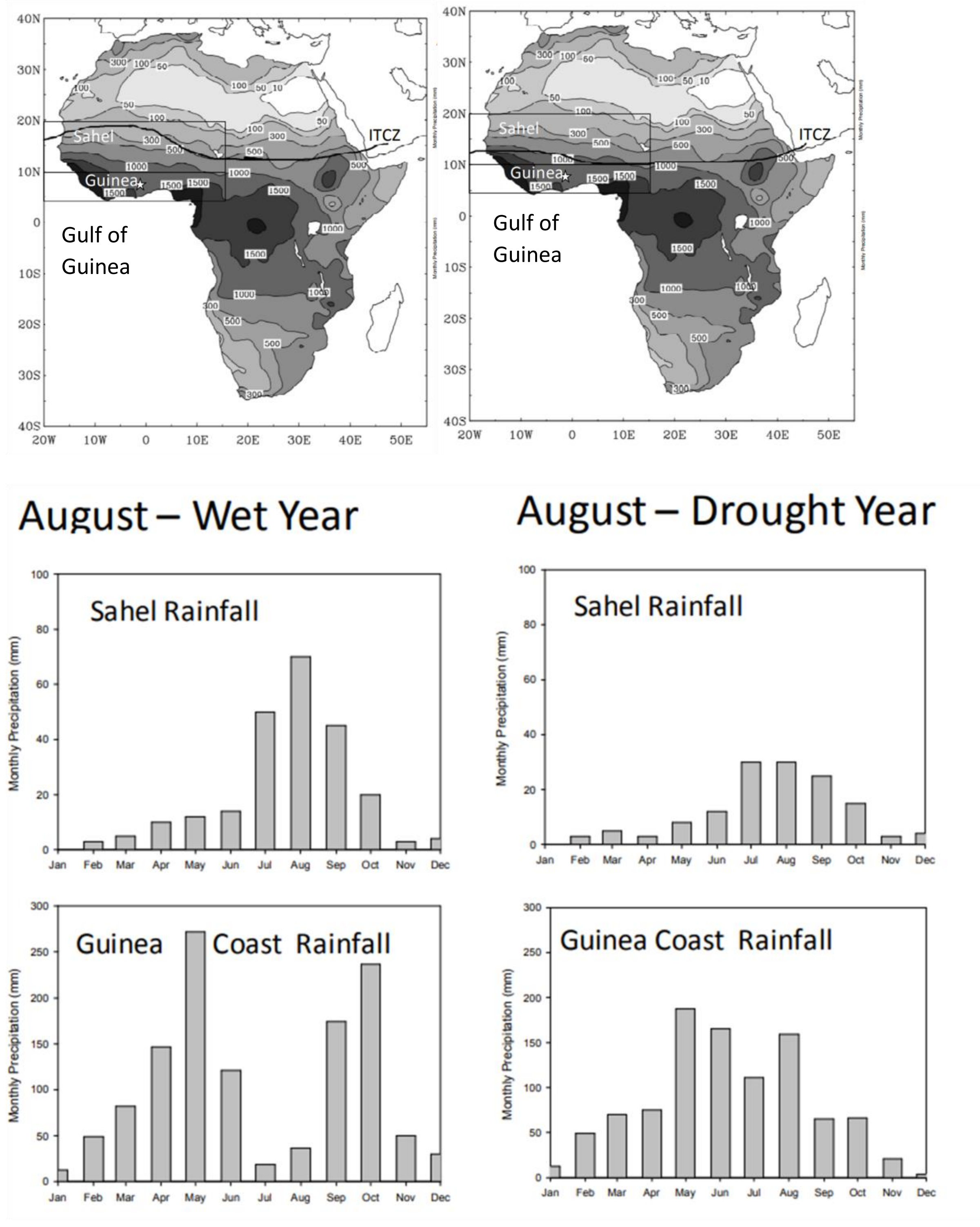

Figure 5. ITCZ position in August and average annual rainfall between wet and drought years for the Guinea Coast and Sahel regions of Africa (Otu et al., 2010).

summer months, June through August. The decrease in precipitation in the summer is due to the upwelling of cold water in the Gulf of Guinea (Fig. 5) from changes in Sea Surface Temperatures (SST) and a more northward migration of the ITCZ from the region. The lowest amounts of precipitation occur in the winter from November through March (Fig.5). The winter or Harmattan season is when the ITCZ is more southward from the lake and the region is strongly influenced by the warm, dry northeasterly trade winds (Gasse et al., 2000; Maley et al., 1991).

B3. *African Humid Period*

During the AHP (~15 to ~5 ka), the ITCZ seasonal wandering was farther north than the present day because of precession conditions, bringing enough rainfall to the Sahara and Sahel region to support the spread of vegetation (Fig. 6) (Shanahan et al., 2019). Water levels in the Nile and many other waterbodies in Africa were considerably higher than present due to increased monsoon strength (Höpker et al., 2019; deMenocal et al., 2000).

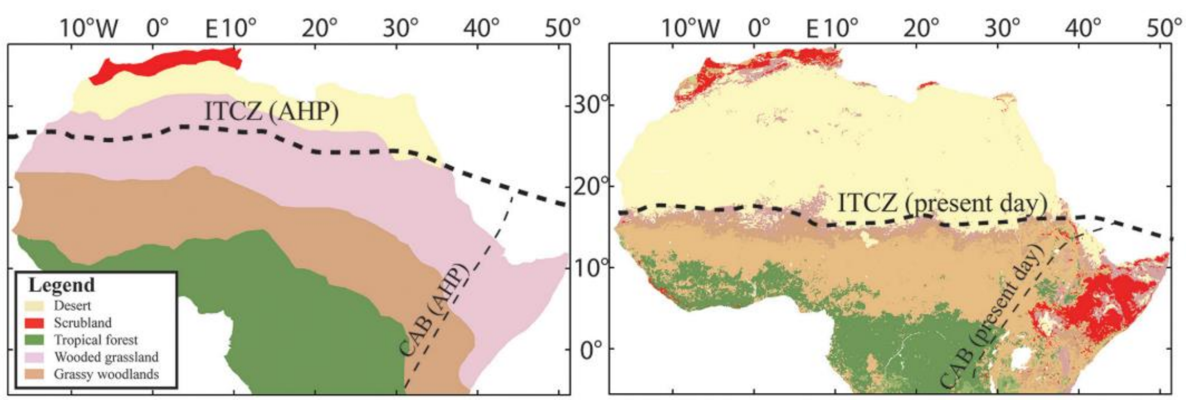

Figure 6. ITCZ and Congo Air Boundary (CAB) summer positioning during the AHP and present-day over northern Africa (Wright et al 2017).

Enhanced monsoon conditions of the AHP are reflected in Mediterranean sapropel deposits derived from Nile River input. The Nile's freshwater influence is evident in Mediterranean sediments by the low $\delta^{18}O$ values measured in planktonic foraminifera and distinct Nd isotope signatures (Scrivner et al., 2004; Rohling et al., 2015). Sapropel is an organic-rich sediment that is indicative of well-stratified water columns and well-established hypolimnion (McGee et al., 2017; Castañeda et al., 2016). As an additional example of increased continent-wide moisture, paleo records of vegetation change at the onset of the AHP ~14 ka suggest a transition from drought tolerant C_4 to C_3 plants. C_3 plants require more moisture than C_4 plants, and C_3 plants were the dominant plant type in north Africa during the AHP (Shanahan et al., 2016).

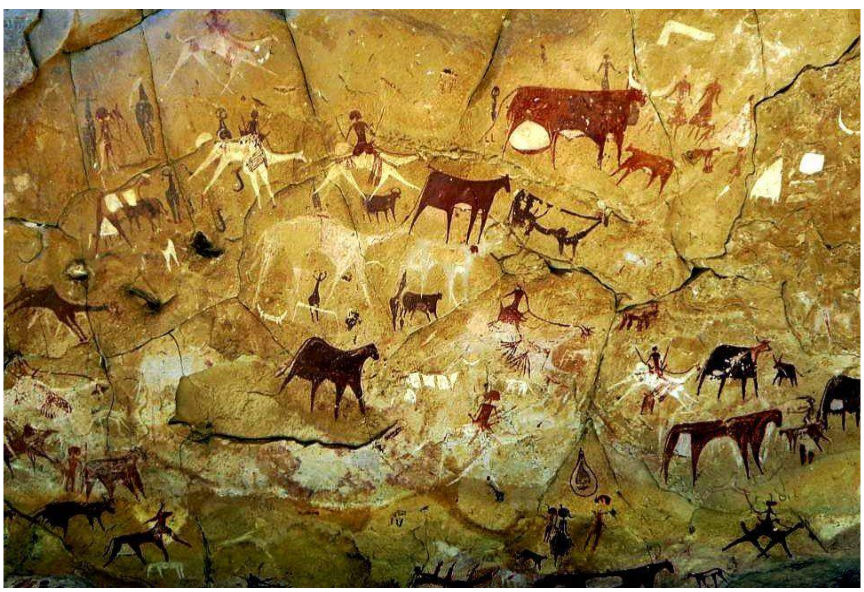

Figure 7. Cave painting of human use of livestock and horses from Manda Gueli Cave northeastern Chad (https://www.archaeology.wiki/blog/2017/03/23/graffiti-scribbled-ancient-cave-paintings-chad/).

Northern Africa's climate was a suitable environment for early human cultivation of crops and the domestication of livestock such as sheep and cattle (Kuper et al., 2006). Examples of flourishing societies are portrayed in cave paintings, which depict a prosperous time for livestock cultivation when the Savanah and Sahel were lushly vegetated (Fig. 7).

The AHP persisted through the middle Holocene, and the maximum insolation occurred during the Holocene Climate Optimum (9.5- 5.4 ka). However, evidence suggests a profound drought during the AHP around 8.2 ka caused by a slowing of the Atlantic thermohaline circulation and decreased rainfall (Gasse et al., 2000). Decreasing northern hemisphere summer insolation from orbital changes weakened the African monsoon cycles and constricted and shifted regions of precipitation between the ITCZ and the CAB more southward (Fig. 6) (Costa et al., 2014).

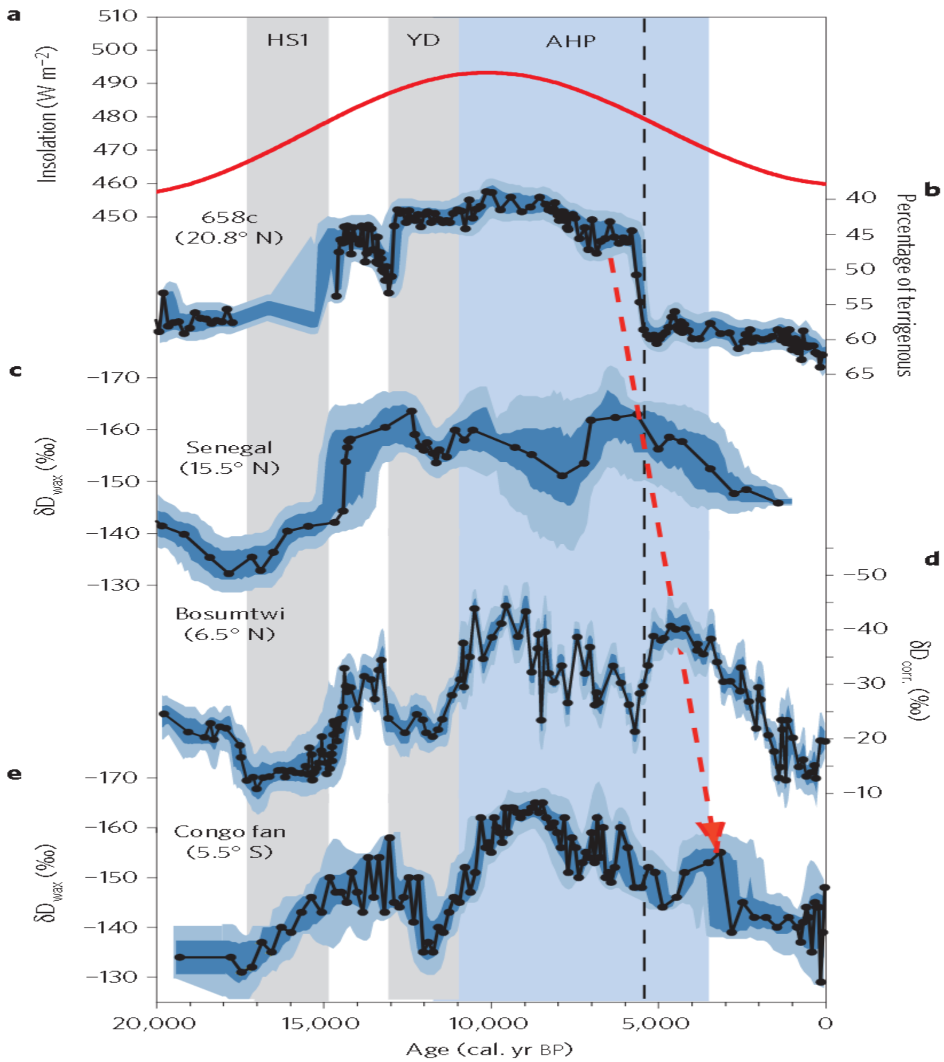

Figure 8. Shifts in climate proxies along low latitudes in Africa over the last 20 ka. (A) Total solar insolation curve at 30°N measured in Wm^{-2} (B) percent terrigenous material from ODP 658-C, (C) leaf wax hydrogen isotopes (δ^2D_{wax}) from Senegal, (D) leaf wax hydrogen isotopes (δ^2D_{wax}) from Ghana (Lake Bosumtwi), (E) leaf wax hydrogen isotopes (δ^2D_{wax}) from the Congo fan The dashed black line represents the termination of the AHP at 5.4 ka and the dashed red line represents transgressive termination of the AHP southwards.

The collapse of the AHP and shift to aridity is earliest seen in the northern and eastern Sahara ~8-7 ka, while regions closer to the equator experience aridity ~5- 3 ka (Fig. 8D, 8E) (McGee et al., 2017; Liu et al., 2017). Lake Bosumtwi in Ghana, west Africa, has provided both magnetic mineral and shoreline highstand evidence that the end of humid conditions occurred around 3 ka as seen in Fig. 3 (Shanahan et al., 2013; Russell et al., 2003; Peck et al., 2004).

B4. Bosumtwi Core Lithology

Lake Bosumtwi sediments have been used for climatic reconstruction (Talbot et al., 1980; Shanahan et al., 2006) because of their high-resolution laminations and continuous deposition. Anoxic bottom water in the lake inhibits bioturbation of sediments, allowing for annual deposition of distinct laminae (Fig. 9).

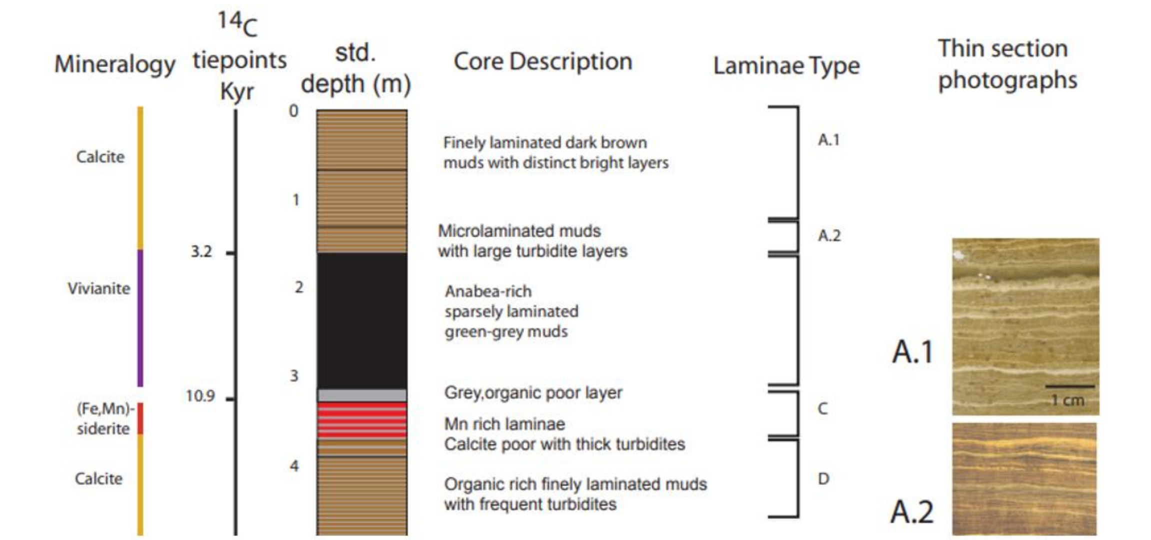

Figure 9. Generalized stratigraphic lithology and descriptions of sediment core from Lake Bosumtwi, Ghana (Shanahan et al 2008).

The period of interest for this study, ~7.4 ka, is confined to the top ~3.4 m of core BOS04-5C. The soft rock drill core used was obtained from Lake Bosumtwi during the GLAD6 coring expedition (Koeberl et al., 2007). The transition at the end of the AHP was marked by a change in lithology, transitioning from poorly laminated, algae-rich sapropel sediment into finely laminated dark brown sediments at roughly 1.7 m (Maley et al., 1991; Abebe., 2010). The bottom 1.5 m of core was poorly laminated, algae-rich sediment or sapropel (gyttja). The sharp boundary between this unit and the overlying unit was representative of the transition between the lake's deep and highly productive state to a shallower lake level (Abebe., 2010). The timing of this transition was dated at ~3.2 ka from calibrated ^{14}C dating of bulk organic matter in the lake sediments. The top ~1.7 m of sediment in the core in Figure 9 was finely laminated muds.

These laminae appear as alternating light brown and dark brown mud. layers. The unit contains 1-2 cm-thick turbidites that appear at the bottom of the section. The lamination of these units can be seen in A.1 and A.2 in Figure 9.

B5. ODP (Offshore Drilling Project) and GeoB offshore sites

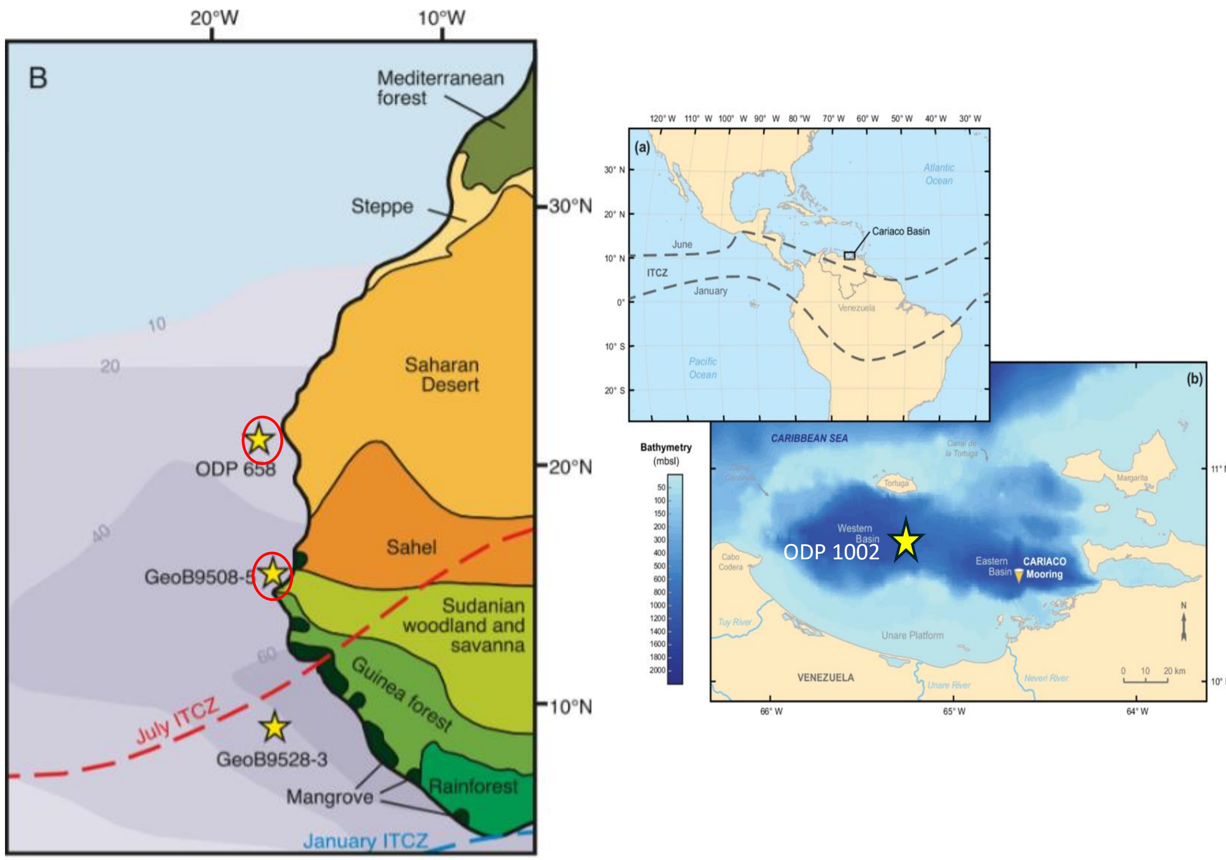

Figure 10. Left - Site locations of ODP 658 and GeoB9508-5 on the NW coast of Africa (Moore et al., 2022) with the major vegetation bands shown. The red dashed line represents the modern summer ITCZ migration. Right- The ODP 1002 site is located in the Cariaco Basin off the northern coast of Venezuela (Bringue et al., 2018)

Marine sediment core data collected from offshore drilling sites along NW Africa and south America (ODP 658, ODP 1002, GeoB 9508-5) were integrated into this project to better understand ITCZ migration at low latitudes (Fig. 10). These offshore datasets were used in this study to highlight precipitation and fire marker abundances in northern portions of Africa compared to the study site (Fig. 2A). The resolution in these data sets is ideal for long-term studies but is limited due to the temporal constraint of this study, with only 10 data points between 8 ka and 1 ka. The south American ODP dataset offers high-resolution hydrological reconstruction through wt.% Ti abundances in sediments. Titanium is a reliable proxy because it is unaffected by post-depositional processes such as diagenesis (Haug et al., 2001; Verschuren et al., 2009)

Core GeoB9508-5

Core GeoB9508-5 (Fig. 10) was collected in 2384m of water, 160 km west of the coast of Senegal (15°29.90'N, 17°56.88'W). The sediment core has been used to reconstruct climate using precipitation proxies (deuterium isotope ratios). The δD data from GeoB 9508-5 (Niedermeyer et al., 2010) were used to reconstruct west African monsoon variability as a function of orbital and millennial changes associated with the hydrological cycle. The δD of C-31 n-alkanes in leaf wax was extracted and measured on a Thermo Trace GC-ULTRA coupled to a Thermo Finnigan Delta$^+$ XP isotope-ratio mass spectrometer.

ODP 658

Ocean Drilling Program (ODP) site 658 is located off the northwest coast of Africa (20.7492°N, 18.5808°W) (Fig. 10) (2263m of water), which is the most northern data set in this study. The sediment from a core at this site has been used to better understand vegetation and climate changes in other periods, such as the Pliocene and Pleistocene (Leroy et al., 1995; Vallé et al., 2014). The charcoal count is represented as a flux that incorporates sediment accumulation rates and bulk density for volume. This dataset also analyzes the percentage of terrigenous material that is deposited offshore, which quantifies how much dust is being produced from the Sahara.

ODP 1002

Marine sediments from ODP 1002 (893 m of water) in Cariaco Basin located off the northern coast of Venezuela (10°42.37'N 65°10.18'W) (Fig. 10), have been used to analyze late Quaternary climate variability, reconstructing migratory patterns of the ITZC and regional hydrology (Peterson et al., 2000, Haug et al 2001).

C. *Proxies of Pyrolysis*

In Lake Bosumtwi, BC was present in sediments in the form of charcoal, soot, and other molecules of pyrolysis (McGee et al., 2017). BC ranges in size from soot aerosols to macro-charcoal particles (>2mm) (Bird et al., 2014). Charcoal is larger than soot and does not travel as far as soot, thus serving as a proxy for local fire activity.

Soot is a form of condensed BC capable of traveling far distances from the original burn location. Soot is formed during condensation of gases emitted during combustion at high temperatures. Soot analysis can be used to reconstruct distal wildfires, while charcoal can reconstruct local wildfires (Kirago et al., 2022).

Levoglucosan and its associated isomers (sugars derived from the pyrolysis of cellulose) are other organic molecular proxies that are useful for identifying lower temperature pyrolysis and changes in vegetation (Tan et al., 2023; Shanahan et al., 2016). The combustion of cellulose and hemicellulose in plants under 350°C produces levoglucosan and its associated isomers (Kuo et al., 2008; Louchouarn et al., 2008). The ratio of the levoglucosan isomers ($C_6H_{10}O_5$) (Galactosan and Mannosan) can be used to identify the source of the vegetation burn. Combustion of softwoods results in Levoglucosan/Mannosan (L/M) and Mannosan/Galactosan (M/G) ratios of (0.7-7) and (0.7-8). The combustion of hardwoods yielded L/M and M/G ratios of (>7) and (>0.7). The combustion of grasses and straws produced L/M and M/G ratios of (>7) and (<0.7) (Tan et al., 2023).

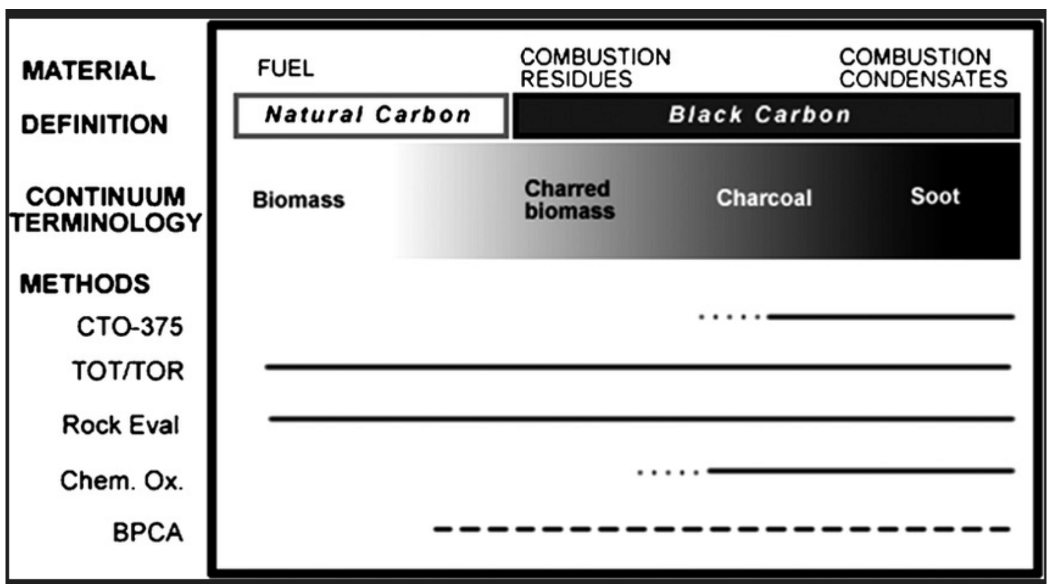

Figure 11. A modification of the combustion continuum depicted in Figure 1 but inclusive of methodological limits. Depicting biomass isolation ranges for Chemo-thermal Oxidation at 375°C, Ratio of Thermal-Optical Transmission to Thermal-Optical Reflectance (TOT/TOR), Rock Eval pyrolysis, Chemical Oxidation and Benzene Polycarboxylic Acid analysis (Poot et al., 2008).

Techniques for isolating each pool of pyrogenic carbon are depicted in Fig. 11. Soot analysis was done using CTO-375 (Hammes et al., 2007). Comparing the ratio between soot aerosols and published charcoal count/concentrations in the sediment core can help us better understand the aeolian transportation of pyrolyzed biomass (Kirago et al., 2022). This could help constrain the timing of aridification in northern Africa at the end of the AHP and compare the heterogeneous termination of the AHP between northern and western Africa.

IV. Methods

Sediments from the top 3.4 m of sediment core BOS04-5C were used for paleoclimate reconstruction in this project. The core was collected in 2004 from lake Bosumtwi in the GLAD4 coring project from the middle/deepest part of the lake. In these sediments, proxies of pyrolysis that serve as wildfire markers will be isolated to deconvolve the fire history in northern Africa. Wildfire markers such as soot and anhydrous fire-derived sugars were isolated using chemo-thermal oxidation and organic extraction, respectively, while charcoal results were reported from other students that optically identified that pool of carbon Gosling et al. (2022). The age(s) of up-core profiles of geochemical variables were quantified using existing age-depth models for each lake (Shanahan et al., 2004, 2015; Peck et al., 2004). Results from the data should enhance the understanding of climatic changes at the end of the AHP between western and northern Africa.

A. Field and Experimental Details

A1. Core Collection, Subsample Calculations

A 3.4m core (BOS04-5C), representing 7.4 ky of sedimentation, was collected during the GLAD6 coring project in 2004 from Ghana's Lake Bosumtwi (6.52227° N, 1.42097° W) (Koeberl et al., 2005). The core samples requested from the University of Minnesota were analyzed at East Carolina University. Core BOS04-5C has a notable change in the rate of sedimentation in depths deeper than 2.1m in the core. To ensure a sample resolution of one sample for every 250 years remained consistent throughout the core, a subsample was taken every 17.5 cm for the upper 2.1 m and a subsample was taken every 5.8 cm for the bottom 1.3 m.

A total of 6 samples were taken for the upper 2.1 m (0m-2.1m) and 23 subsamples were taken for the bottom 1.3m of the core (deeper than 2.1m), for a total of 29 lake samples.

A2. *Lake Bosumtwi Age-depth model*

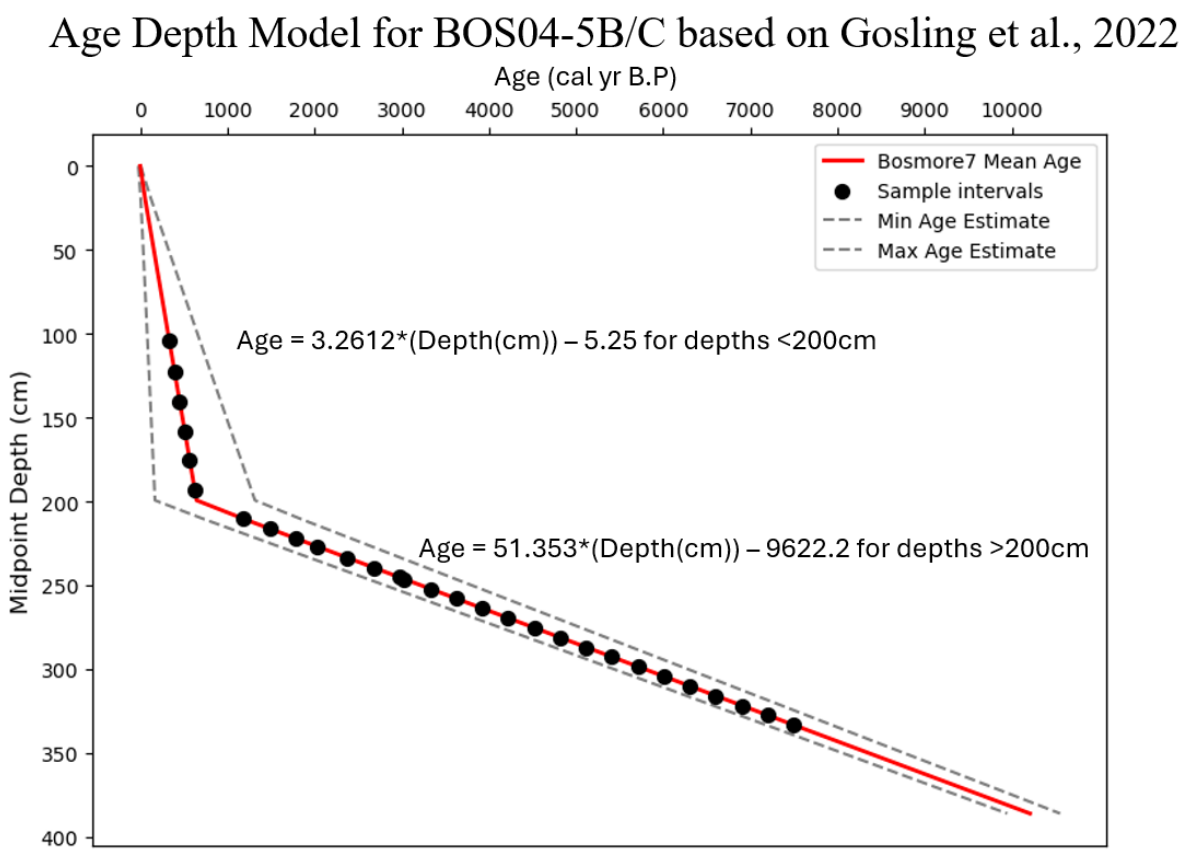

Figure 12. The age-depth model was established from BOSO-5c and 5b cores, referred to as BOSMORE7 in Gosling et al., 2022. The red line plots the BOSMORE7 multi-dating approach, the C^{14} ages were derived from fish skeletons and bulk organic sediments, and dashed grey lines represent the minimum and maximum ages computed by BOSMORE7. The black dots show extrapolated ages based on linear fits before and after 200cm, with their associated linear equations on the bottom right.

The age model used in this study was linearly extrapolated from ages produced by the BOSMORE7 (Gosling et al., 2022) age-depth model (Fig. 12) for BOS04-5B and 5C cores (Fig. 13), which utilizes Bayesian statistics to model the multi-dating approach. The model uses AMS C^{14} dating for bulk sediments and collagen in fish skeletons in younger sediments, utilizing optically stimulated luminescence and uranium-thorium ages for older sections of the core. A distinct change in sedimentation can be seen at ~200 cm (Shanahan et al., 2013).

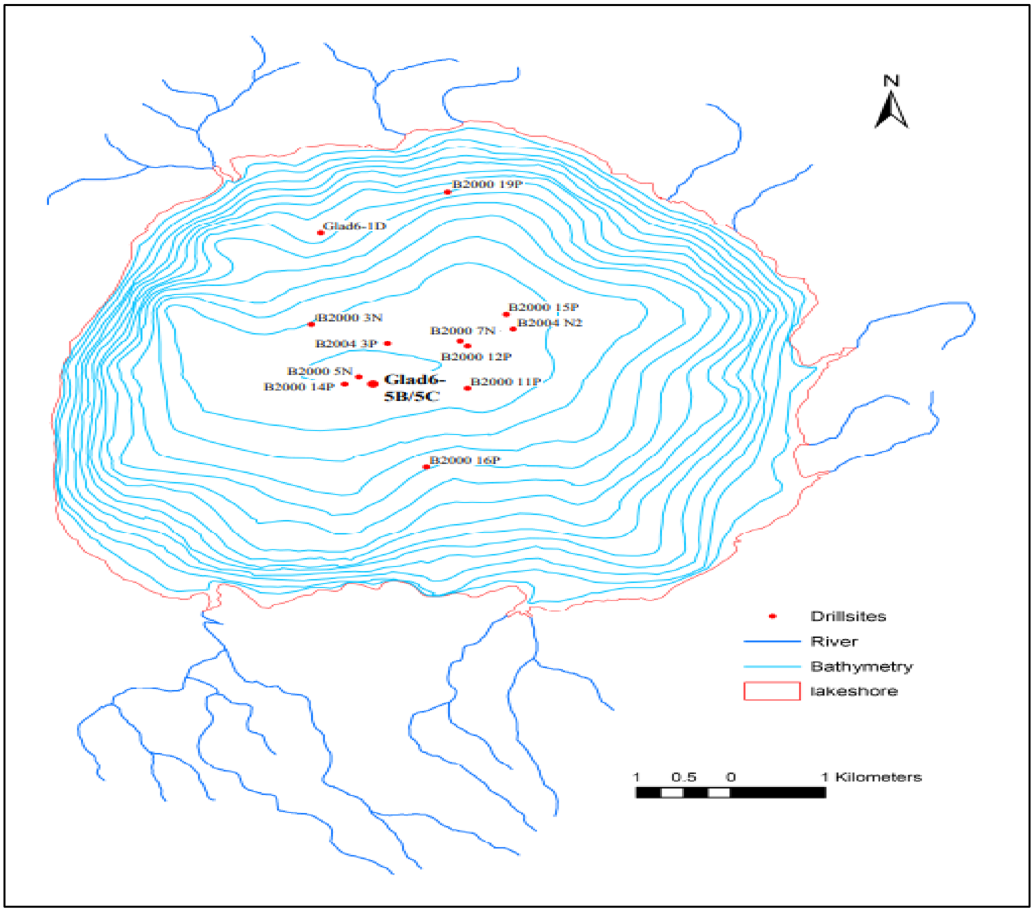

Figure 13. Bathymetry and locations of core collection sites and Glad6-5B/5C in Lake Bosumtwi (Abebe et al 2010).

A3. Sediment Geochemistry

Total Organic Carbon (TOC) isolation

In TOC isolation, one gram of dried homogenized bulk sediment was moved to a clean scintillation vial and treated with 2N HCl iteratively to remove carbonate material. Each addition of HCl was administered until the effervescing stopped. Samples were left to soak for 24 hours in 2N HCl to ensure all carbonate removal. The samples were rinsed with distilled deionized (DDI) water 3 times, and the supernatant was tested for acidity using litmus paper until it reached a pH of 7. The samples were then placed in the heating oven at 66°C. Sample masses were recorded every day upon placement in the oven until there were no changes in individual sample masses.

Carbon and Nitrogen analysis

Samples for carbon, nitrogen, and soot abundance and bulk isotopic composition (TOC%, $\delta^{13}C_{TOC}$, TN%, $\delta^{15}N$, and C_{Soot}%, $\delta\ ^{13}C_{Soot}$) quantification were gravimetrically placed in tin capsules, crimped, and then sent to the Stable Isotope Lab at the University of Florida. Samples were loaded onto a 50-position automated Zero Blank sample carousel on an N.C. Technologies ECS 8020 elemental analyzer. After combustion in a quartz column at 1000°C in an oxygen-rich atmosphere, the sample gas was transported in a He carrier stream and passed through a hot reduction column (650°C) consisting of elemental copper to remove oxygen. The effluent stream then passed through a chemical (magnesium perchlorate) trap to remove water, followed by a 1.5-meter GC column at 55°C to separate N_2 from CO_2. The sample gas was next passed into a ConFlo IV interface and into the inlet of a Thermo Electron Delta V Advantage isotope ratio mass spectrometer running in continuous flow mode, where the sample gas was measured relative to laboratory reference N_2 and CO_2 gases. All carbon isotopic results are expressed in standard delta notation relative to VPDB (Vienna Pee Dee Belemnite). All nitrogen isotopic results are expressed in standard delta notation relative to air.

Levoglucosan isomer extraction

Sample sediments were dried and extracted with a solution of acetone and hexane in a 1:1 ratio by volume. The samples were then spiked with 0.1mL of C^{13} labeled levoglucosan as an internal standard before being extracted to gauge the recovery of analytes during extraction. The samples were then agitated via sonication for 15 minutes using a Fisher Scientific Ultrasonic Cleaner model FS20. The samples were then centrifuged for 5 minutes at 500 rpm, after which the supernatant was removed and transferred to a rotovap (rotary evaporation) flask. This process was repeated 3x for each sample. Samples that had high turbidity after being centrifuged were then filtered using pre-combusted (450 °C for 4h) glass wool loaded into a Pasteur pipette, followed by ~3 inches of pre-combusted $NaSO_4$, and capped with another tuft of glass fiber wool. The pipette-filter GFF was pre-rinsed with the clean extraction solvent. The supernatant was then concentrated dryness in the rotovap. A small amount of pyridine was placed in the rotovap flask and rinsed along the inside walls to minimize recovery. A subsample of the samples in pyridine were derivatized with [bis (trimethylsilyl) trifluoroacetamide] (BSTFA) at a (1:1) ratio. Samples were cooled sufficiently before being transferred into a GC-MS vial with hexane and injected into a GC-MS for analysis.

V. Results and Discussion

A. Bulk elemental abundances

TOC

Changes in bulk elemental abundances such as TOC are due to factors such as regional influx of organic matter via runoff throughout the watershed into Lake Bosumtwi, post-depositional microbial activity, and distal inputs such as aeolian deposition. The whole core TOC (Fig. 14A) averaged 10.36 ± 0.78%. The highest abundance can be seen at 5.1 ka and the period between 2.3 ka and 1.4 ka, indicating episodic increases in biomass input. At the end of the AHP (7.4 ka to 5 ka), the TOC was the highest at 10.6 ± 0.7%. During this time, TOC decreased from ~12% to ~7% from 7.4- 7.2 ka, then gradually increased to ~16% at 5.1 ka (post-AHP).

The average post-AHP TOC (5 ka to 0.3 ka) was 10.07 ± 0.86%. Around the end of the AHP at 5 ka and around 2.9 ka (post-AHP), there are shifts in TOC deposition. At 4.8 ka, the TOC decreases to 6%, which could be reflective of a weakened summer monsoon system. Between 5 - 3.2 ka averaged 9.1%; however, this decrease in TOC coincides with periods of increased precipitation (Fig. 16B). A shift in TOC at 2.9 ka coincides with the termination of the sapropel layer, the TOC decreasing from 11.5% to 2.5%.

The δ^{13}C of organic carbon ($\delta^{13}C_{TOC}$) has historically been used to discriminate sources of biomass between C_3 and C_4 plants via their photosynthetic pathways. The δ^{13}C of C_4 plants (grasses) falls between -16‰ and -10‰, while C_3 plants (hardwoods) have a range of -34‰ to -22‰ (O'Leary 1988). The $\delta^{13}C_{TOC}$ in BOS04-5C (Fig. 14A) shows a generally depleting trend from 7.4 ka, with an upcore average of -25.51‰. At the end of the AHP (7.4 ka to 5 ka), the average was -22‰ and follows a depleting trend between 6 ka and 5.1 ka. Post-AHP, there was an enrichment between 5.1 ka and 3 ka, increasing from -26.88‰ to 21.94‰, indicating an increase in the deposition of C_3 plants. Afterwards, there was an abrupt and sizeable isotopic shift at 3 ka, decreasing from -21.93‰ to -29.44‰ at 2.9 ka, suggesting greater deposition of C_4 plants. The upcore plot shows a decrease in the deposition of C_3 plants between 7.4 ka and 5.1 ka, a gradual increase in C_3 deposition between 5 ka and 3 ka; before shifting to more deposition of C_4 plants between 2.9 ka and 0.33 ka.

C_{soot}

The upcore average percentage of C_{Soot} (Fig. 14B) was 0.16 ± 0.03 %, showing a general decline in soot carbon since the peak of 0.6% at 7.2 ka. At the end of the AHP, the C_{Soot} was 0.21% ± 0.079. There was relatively higher soot deposition seen at 7.2 ka, 6.6 ka, and 5.7 ka with values of 0.60%, 0.36%, and 0.39%, respectively. Post-AHP, the C_{Soot} also averaged 0.14 %. An increase in C_{Soot} was observed at 3.9 ka at 0.26%. There were other notable peaks at 2.6 ka, 1.1 ka and 0.39 ka, with values of 0.2%, 0.22% and 0.53%, respectively.

Both soot and levoglucosan isomers are fire proxies that are subject to aeolian transport via the ITCZ and trade wind dynamics, however, soot is formed at much higher combustion temperatures than levoglucosan. Trends in C_{Soot} and sugar isomers are similar throughout the core. Furthermore, levoglucosan isomers and soot both show higher abundances between 7.3 ka and 5.1 ka compared to post-AHP abundances (Fig. 14E). C_{Soot} and levoglucosan isomers decreased in abundance between 5.1 ka and 3 ka compared to older periods. This decrease could be due to limited biomass availability in northern Africa at the end of the AHP or increases in precipitation as seen in the δD record from GeoB 9508-5 (Fig. 16B) (Moore et al., 2022).

The $\delta^{13}C_{Soot}$ (Fig. 14B) had an average $\delta^{13}C_{Soot}$ of -24.96‰, the trend mimics the $\delta^{13}C_{TOC}$ with a distinct isotopic shift at 3.2 ka.

At the end of the AHP (7.4- 5 ka), the average $\delta^{13}C_{Soot}$ was -21.34‰ ± 0.22, with the most enriched samples of -15.32‰ seen at 7.2 ka. The plot also follows an upcore depletion with periods of slight enrichment between 6.6 ka and 5.1 ka, averaging at -22.9‰. The plot shows a gradual depletion to -26.22‰ from 5.1 ka to 4.2 ka. This was followed by a gradual enrichment until 3.0 ka, when a significant depletion shift from –20‰ to –28‰ occurs.

The depletion in the carbon isotope signatures of soot isolated samples reflects changes in biomass combustion source, suggesting a relative decrease in the combustion of C_4 (grasses) compared to C_3 (hardwoods) plants between 7.4 ka and 3 ka. Between 5 ka and 3.2 ka, the isotopic range was more depleted compared to during the AHP, but gradually enriched approaching 3 ka. At 2.9 ka, an abrupt shift in $\delta^{13}C_{Soot}$ reflects a change in combustion sources, which is indicative of more C_3 hardwood plants (O'Leary 1988).

TN

Changes in TN% (Fig. 14C) in the lake reflect different nutrients derived from allochthonous inputs, such as runoff or autochthonous (nitrogen-fixing) processes in the lake's watershed. The plot depicts the total upcore nitrogen in core BOS04-5C; the average TN is 6% ± 0.06. At the end of the AHP, the TN averaged 0.54% ± 0.05. The lowest TN is 0.39% and occurred at the end of the AHP occurred at 7.2 ka. Post-AHP, TN was 0.63 ± 0.07%. An increase in TN can be seen from 0.49% to 0.83% and then decreased to 0.29% between 5 ka and 2.6 ka. The relatively elevated total nitrogen abundance between 7.4 ka and 5 ka reflects a more productive water column; elevated TOC, δD (Fig. 16B, and lake reconstruction highstand (Fig. 3C) also suggest wetter periods with increased precipitation. The end of the AHP in lake Bosumtwi is apparent in core lithology at ~3 ka or ~2.5m, depicted as a transition from organic rich mud (sapropel) into finely laminated sediments. A distinct shift in numerous analyses (TOC,

$\delta^{13}C_{TOC}$, $\delta^{13}C_{Soot}$ TN and C/N) occurred around 3 ka, which coincides with the end of the sapropel layer.

The stable isotopic signature of nitrogen post-burial can be influenced by microbial processes in situ. There was a significant shift of ~9‰ within TN that occurred between 3 ka and 2.9 ka, shifting from 14.29‰ to 5.8‰, concurrent with shifts seen in $\delta^{13}C_{TOC}$ and $\delta^{13}C_{Soot}$. $\delta^{15}N$ (Fig. 14C) then shows an oscillating trend with periods of relative enrichment occurring at 1.7 ka to 1.4 ka, 0.56 ka, and 0.39 ka, with averaged isotopic ranges of 9.38‰, 9.89‰, and 8.7‰, respectively. The upcore trends in $\delta^{15}N$ are distinctly different compared to the upcore trends $\delta^{13}C_{TOC}$. The upcore average for $\delta^{15}N$ was 10.22‰ ± 0.5. Sediments were more enriched in $\delta^{15}N$ between 7.4 ka and 5 ka compared to sediments younger than 5 ka. At the end of the AHP (7.4- 5 ka), $\delta^{15}N$ is 12.9‰, while the average Post-AHP is 9‰. Between 7.4 ka and 5.4 ka (near the end of the AHP), nitrogen appears to have a notably depleted isotopic signature. This was followed by more isotopic enrichment with an average of 14.49‰ between 6 ka and 5.1 ka. There was another period of depletion that occurred at 4.8 ka, followed by an enrichment between 4.5 ka and 5 ka with an average of 12.5 ‰.

In other sediment cores from Lake Bosumtwi (B6 and B7; Talbot et al., 1984), a transition from sapropel to calcareous laminated muds can be seen at 210cm with a distinct +4‰ shift in $\delta^{15}N$ (Russell et al., 2003; Talbot and Johannessen, 1992). In BOS04-5C, a significant shift in $\delta^{15}N$ was seen at 246cm or 3 ka. In Talbot and Johannessen et al. (1992), the $\delta^{15}N$ in the AHP sediments was more depleted, averaging ~4‰, while samples from BOS04-5C averaged 12.5‰. The low $\delta^{15}N$ in sediments was explained by a dominant input from cyanobacteria via N-fixation. The heavier values seen after the termination of the sapropel layer were explained by a shift into heterotrophic N sourcing (Russell et al., 2003). This difference in the $\delta^{15}N$ between cores could be attributed to post-coring mold growth during storage. The nitrogenous components of organic matter are more labile than carbon and are more susceptible to decomposition, which can alter the abundance and isotopic composition (Lee et al., 1984).

TOC/TN

TOC/TN ratios have historically been used to differentiate organic matter sources from terrestrial/allochthonous vs autochthonous (Meyers et al., 1993). Organic nitrogen is used in the production of proteins and nucleic acids by aquatic organisms such as phytoplankton and bacteria (Lee et al., 1984). Thus, organic matter produced in the water column (autochthonous) has a low TOC/TN ratio in ranges of <10. Terrestrial plants that use lignin and cellulose in their structures are typically nitrogen-poor (Lee et al., 1984) and therefore have a higher TOC/TN ratio (>20).

The TOC/TN molar ratio has a whole core average of 17.4 (Fig. 14D). It shows a fluctuating pattern between 7.4 ka and 3 ka with an average ratio of 20.9 and then shifts significantly after 3 ka. Between 7.4- 5 ka, the average TOC/TN was 20.04, ranging from 19.54 at 7.4 ka to 25.90 at 5.1 ka. The ratio then increased and averaged at 22.5 between 5 ka and 3 ka. After 3 ka, the ratio decreases significantly from 19.98 to 8.62 at 2.6 ka. The ratio then increases in younger sediments, averaging at 13.32 between 2.3 ka and 0.33 ka. The upcore ratio highlights a transition to organic matter sources in the lake's water column: the ratio decreases to values averaging at 13 from 3-0.3 ka, from an average of 21 between 7.4- 3 ka. This transition highlights a shift in organic matter sources, showing the predominance of allochthonous nutrient input between 7.3 ka and 3 ka, and increased autochthonous productivity after 3 ka.

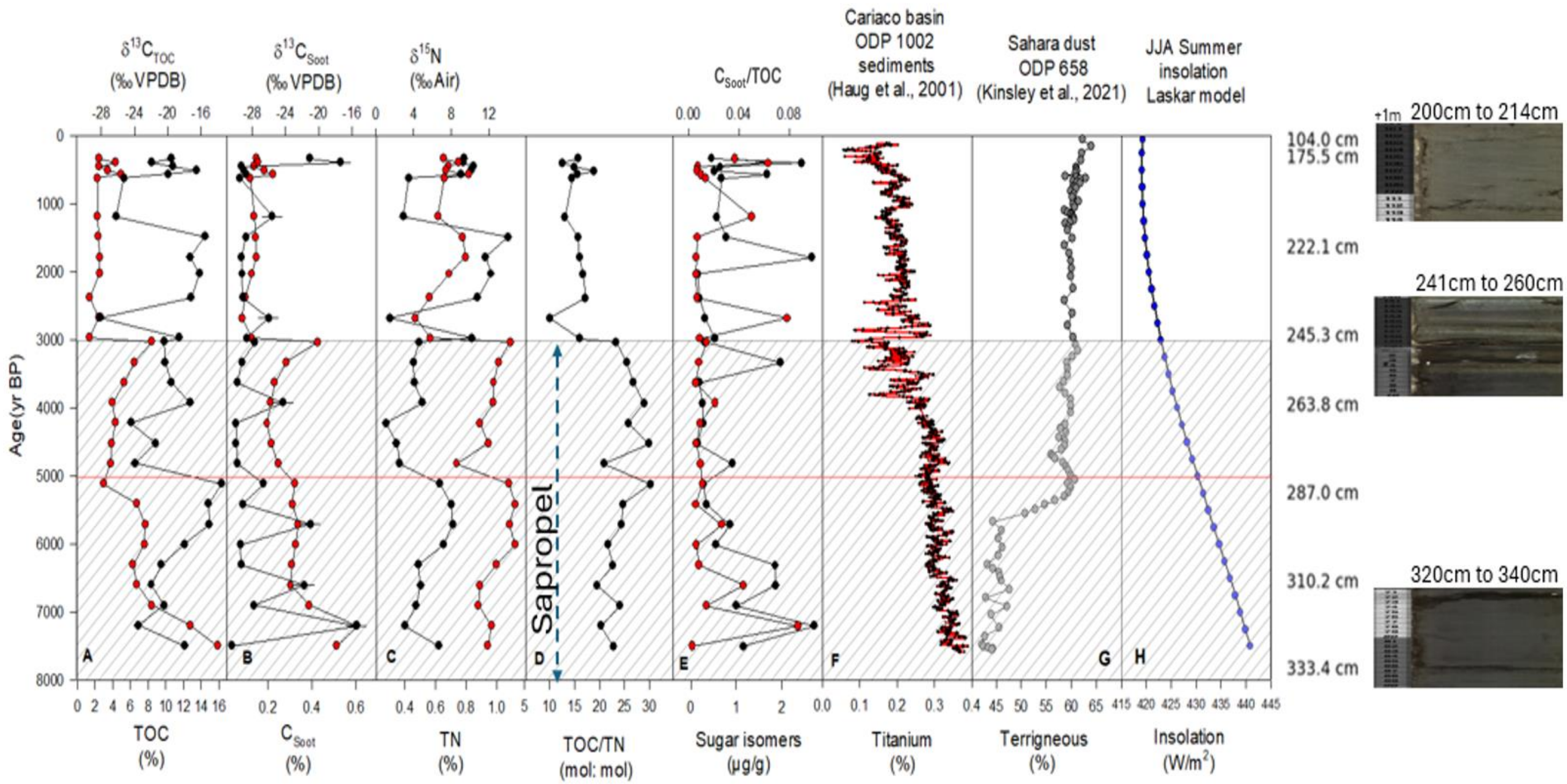

Figure 14. (A) Upcore TOC% of bulk sediment (●) plotted in black and TOC isotopic range ($\delta^{13}C_{TOC}$) expressed in permille, VPDB plotted in red (●) (B) C_{Soot} % plotted in black (●) and stable isotopic signature of C_{soot} (permille VPDB) plotted in (●) (C)Total nitrogen plotted in black (●)and isotopic range of nitrogen expressed in permille, Air plotted in red(●) (D) molar ratio of total organic carbon to total nitrogen (E) The upcore concentrations of the sum of sugar isomer expressed in µg/g in black (●) with $C_{Soot/TOC}$ plotted in red(●), (F) Ti% from Cariaco basin ODP-1002 as a proxy for rainfall (Haug et al. 2001). (G) The proportion of terrigenous material found offshore in the sediments of ODP 658-C. (H) The mean summer insolation at 6°N expressed in W/m^2 Midpoint depths for BOS04-5c and core images at select depths plotted on the right side of the graphs. The red line at 5 ka represents the end of the AHP in northern Africa and the greyed area below 3 ka represents the sapropel layer

B. Trends in Fire Proxies

Sugar concentrations and proportions

The upcore concentrations of levoglucosan (Fig. 15A) averaged 0.36µg/g and show an increase in sugar concentrations post-AHP. At the end of the AHP (7.4 – 5 ka), levoglucosan had an average concentration of 0.48µg/g, with the highest concentration of 1.13µg/g occurring at 6.6 ka. The concentrations sharply decline throughout the rest of the AHP, averaging 0.27µg/g between 6.3 ka and 5 ka. Post-AHP, a general decrease in levoglucosan concentration can be seen between 5 ka and 3.6 ka with an average of 0.15µg/g. Near the 3 ka boundary, there was an increase in concentration from 0.01µg/g at 3.6 ka to 0.5µg/g at 3.3 ka.

Mannosan (Fig. 15B) had the highest average concentration at 0.49µg/g. The highest mannosan concentration occurred at 7.4 ka with a concentration of 2.22µg/g. At the end of the AHP, the concentration averaged 0.67µg/g. Increased periods of mannosan deposition exceeding 1.4µg/g were observed at 7.4 ka and 6.3 ka. Post-AHP, the concentrations average 0.46µg/g, with the highest concentration at 1.7 ka with 2.02µg/g.

Galactosan (Fig. 15C) had the lowest average concentration among the sugar isomers at 0.025µg/g with a maximum concentration at 2.6 ka with a value of 0.16µg/g. At the end of the AHP, the sugar concentration averaged 0.024µg/g. During this time, the highest concentration occurs at 6.6 ka with a value of 0.09µg/g. Post-AHP, the average decreases slightly to 0.02µg/g with the highest concentration at 2.6 ka. However, the lowest concentration can be seen between 5 ka and 3.2 ka with an average of 0.018µg/g.

In the sum of the concentrations of sugar isomers (Fig. 15D), levoglucosan, mannosan, and galactosan, there was an average concentration of 0.91µg/g ± 0.19. At the end of the AHP, there was a slightly higher average concentration of 1.18µg/g, compared to the Post-AHP average of 0.78µg/g, which continues until 0.33 ka when the concentrations increase to 2.66µg/g at 0.39 ka. There were 3 other distinct periods of increased sugar concentrations at 3.3 ka, 1.7 ka, and 0.39 ka with concentrations of 1.97µg/g, 1.68µg/g, and 2.45µg/g, respectively.

The proportions of isomers extracted in relation to the TOC (Fig. 15) from the BOS04-5C core showed higher concentrations of levoglucosan and mannosan when compared to galactosan. Common features between the isomers were the increased abundances seen at 7-6 ka, and 3-2.5 ka, with decreased concentrations between 5 ka and 3 ka, aligning with the weakened monsoon activity.

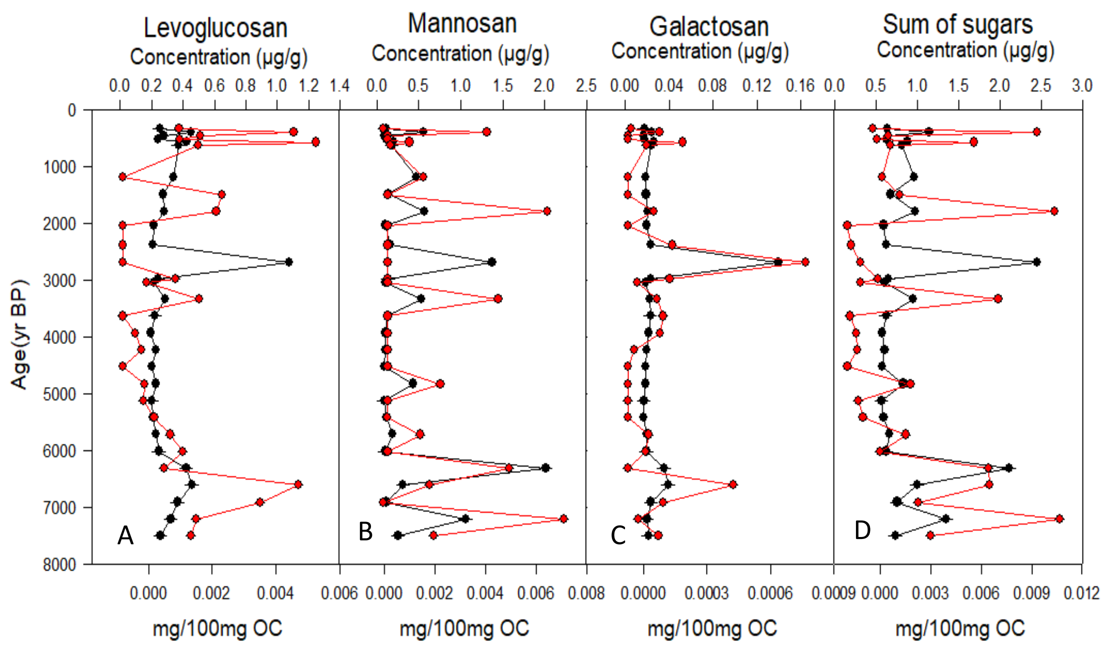

Figure 15. (A) Upcore concentration and proportion of levoglucosan to TOC in µg/g plotted in red (●) and mg/100mg TOC plotted in black (●), (B) Concentration and proportion of mannosan in µg/g plotted in red (●) and mg/100mg TOC plotted in black (●), (C) Concentration and proportion of galactosan plotted in red (●) and mg/100mg TOC plotted in black(●) (D) Sum of sugars concentration and proportion in µg/g plotted in red (●) and mg/100mg TOC plotted in black (●).

C. Holocene Paleoclimate Forces Affecting Wildfire Activity in northern Africa

Trends in markers of pyrolysis in Core BOS04-5C and ODP sites can be driven by regional factors such as anthropogenic biomass burning, changes in vegetation, or synoptic climatic forcing. Wildfire activity in northern Africa is recorded in sediment records as increased deposition of soot or charcoal relative to the total organic carbon content.

The C_{Soot}/ TOC ratio distinguishes carbon sources between local and distal pools. As noted earlier, soot is a refractory form of carbon that is formed from the condensation of pyrogenic gases and has the potential for aeolian transport due to its size. Increased deposition of soot compared to TOC indicates relatively greater influx of pyrogenic material from aeolian processes. Like the other proxies for pyrolysis, a greater abundance of soot was seen at the end of the AHP and after the termination of the sapropel layer at 3 ka. The trend also shows lower abundances of C_{Soot}/TOC between 5 ka and 3 ka with increased abundance in modern sediments. The increased ratio of C_{Soot}/TOC during the AHP suggests an increase in aeolian soot transport from the Sahara.

I use charcoal counts from BOS05B/5C to interpret local fire activity around the lake's watershed (after Gosling et al., 2022). The data show a lower abundance of charcoal between ~7 ka and 4 ka at ~20,000 particles per cm^3. However, an increase can be seen between 4 ka and 3 ka, increasing to ~80,000 particles per cm^3 (Fig. 16E). This increase in fire activity at 3 ka may reflect a weaker monsoon input unable to suppress local wildfire activity in the winter months as the ITCZ moved north of lake Bosumtwi (Haug et al., 2001; Shanahan et al 2015; Gosling et al., 2022). At higher latitudes, the charcoal flux from ODP 658 (Fig. 16D) (Moore et al., 2022) highlights a decreased abundance of charcoal during the AHP, with a slight increase in abundance at 6.7 ka. The data suggests a suppression of fire activity around 5 ka, similar to the C_{Soot} and levoglucosan isomer trends in the Bosumtwi data.

Middle-late Holocene trends in our data around 3 ka may result from global climatic forcing, such as migration of the ITCZ. A synchronous record of the southward migration of the ITCZ around 5 ka from south America is consistent with changes seen in the northern African climate (Russell et al., 2003). The Ti% decrease around this time suggest a strong ENSO input which starts around 5 ka. ENSO events have historically weakened trade winds and altered the ITCZ migratory path as observed in modern periods of Sahelian drought in the 1980s (Janicot et al., 1996).

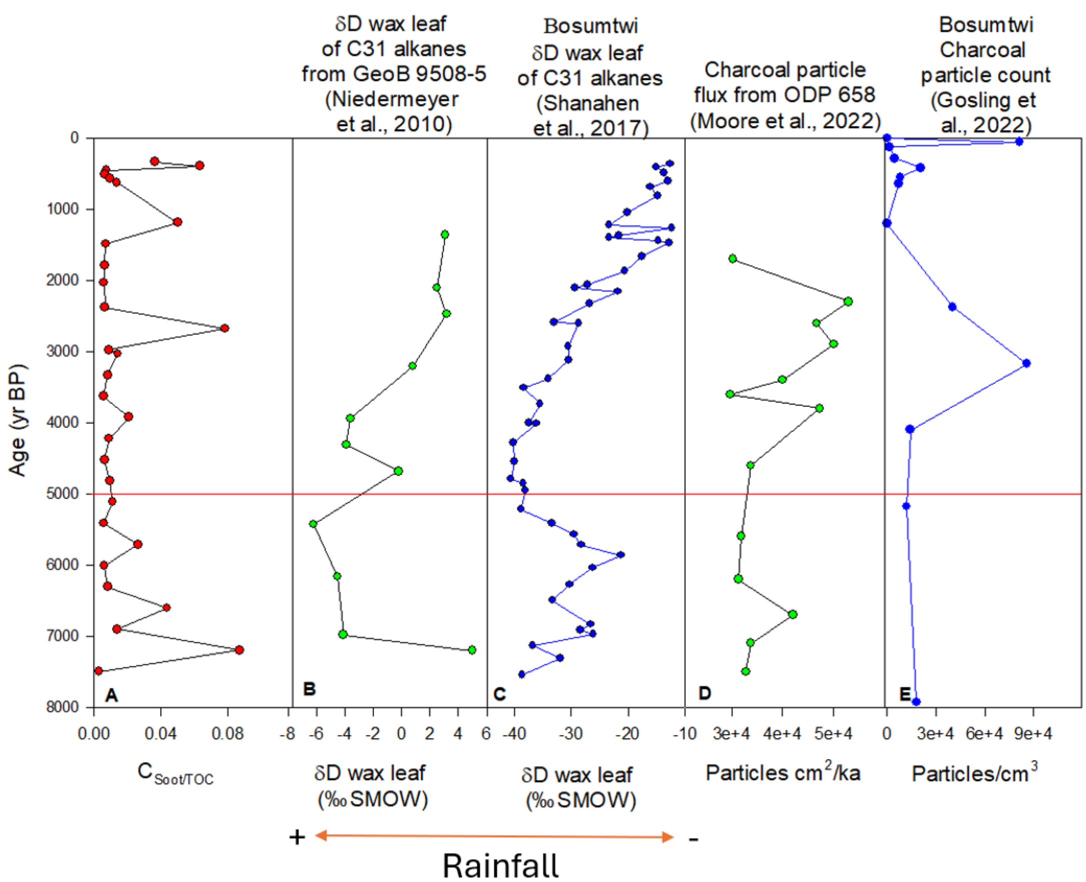

Figure 16. (A) Upcore $C_{Soot}/_{TOC}$, (B) δD of wax lead of C-31 n-alkanes expressed in permille, SMOW from GeoB 9508-5 (15°N, 17°W) (Niedermeyer et al., 2010). (C) δD of wax leaf C-31 n-alkynes expressed in permille Standard Mean Ocean Water (SMOW) corrected for ice volume (Shanahan et al., 2015), (D) Charcoal particle flux expressed in cm^2/ky from ODP 658 (21°N, 19°W) (Moore et al., 2022). (E) Charcoal counts in particles per cm^3 from BOS04-5b Gosling et al., 2022

D. Interpreting hypotheses

Hypothesis 1

H1: A southward migration of the ITCZ led to drought conditions and change in vegetation through much of northern Africa, eventually leading to the end of the AHP. In this study we predicted that elevated concentrations of pyrogenic organic matter should be present in the sedimentary record of Lake Bosumtwi preceding drought periods at the termination of the AHP.

The elevated abundance of pyrogenic organic matter (C_{Soot} and levoglucosan isomers) between 7.4 ka and 5 ka suggests increased wildfire activity as northern Africa transitioned into its current hyper-arid state. The decrease in pyrogenic organic matter after 5 ka supports this hypothesis as the biomass availability decreased and erosion from the Sahara increased, as seen in Fig. 14G

Hypothesis 2

H_2: The ratios of aeolian soot to charcoal in downcore sediments of Lake Bosumtwi, Ghana, provide evidence of drought conditions in the Sahara and Sahel regions of northern Africa. In this study, we predicted that elevated proportions of soot to charcoal in Bosumtwi sediments should reflect an increase in distal wildfires before the termination of the AHP in northern Africa.

The trends of regional drought (Fig. 16. B, C) and local fire activity (Fig. 16. D, E) are dissociated from the C_{Soot} trends. The dissimilar trends suggest that the C_{Soot} deposition is unrelated to locally produced black carbon from wildfires. Based on the current understanding of the prevailing wind directions of the present day ITCZ and its migration history, the C_{Soot} is likely originating from the interior of northern Africa.

Hypothesis 3

H3: The $\delta^{13}C$ values of pyrogenic organic matter in sediments can be used to distinguish the source of the biomass that was combusted. In this study, we predicted an increased abundance of C_3-derived pyrogenic organic matter between 7.4 ka and 5 ka, followed by an increase in C_4-derived pyrogenic after the termination of the AHP.

My findings did not support this hypothesis, as there was an increase in the combustion of C_4-derived material relative to C_3-derived material between 7.4 ka and 5 ka. Post-AHP, the isotopic ranges were more depleted between 5 ka and 3 ka, suggesting increased relative combustion of C_3-derived material relative to C_4-derived material. These results were contradictory to the expectations of the third hypothesis. This could be due to the distribution of the abundances of C_3 and C_4 in the Sahara and Sahel regions. C_4 vegetation may be more prone to desiccation in drought conditions due to limited soil moisture accessibility; however, they may also be more likely to succeed (produce viable offspring) in arid conditions (Taiz et al., 2015) and increase the availability of biomass for combustion.

IV. Conclusions

The proxies for pyrolysis (C_{Soot}, sugars isomer concentrations, charcoal particles, and C_{Soot}/TOC) generally support hypotheses H1 and H2. The post-AHP weakened monsoon in northwestern Africa is evident in the decrease in TOC, TN, and δD around 3 ka. The decrease in Ti% since the Holocene Thermal Maximum illustrates the southward migration of the ITCZ, coinciding with the periods of increased abundance of pyrogenic markers. C_{Soot} and sugars isomers show an increase in abundances leading up to the end of the AHP, which supports H2. C_{Soot} and sugar isomers were less abundant in the period between 5-3 ka, while charcoal count peaked at 3 ka. After 3 ka, the fire markers are generally less abundant but increased universally in modern sediments around 0.5 ka. H3 proved to be contrary to our findings; there was increased combustion of C_4 plant material between 7.4 ka and 5 ka. Initially, we hypothesized there would be more C_3 combustion since C_4 plants are more drought tolerant; however, the relative distribution in abundance of these vegetation types could play a significant role in the abundances of black carbon produced. Meaning, while C_3 plants are less adaptive to drought conditions making them more susceptible to wildfires, their isotopic signature may be muted by the higher abundance of combustible C_4 plant biomass.

Some uncertainties can be seen in the carbon composition data sent to UF for analysis. There are considerable deviations in both C_{Soot}% and $\delta^{13}C_{soot}$ between replicates of soot samples sent off. This could potentially be due to a failure or inefficient homogenization of samples post CTO-375; the replicate batches were adequately homogenized before crimping. Other uncertainty lies in the similarity of $\delta^{13}C_{Soot}$ and TOC $\delta^{13}C$, though the abundances vary, it was less apparent in the isotopic ranges. The similarities call into question the sourcing of soot (local or distal). The TOC $\delta^{13}C$ is also notably distinct from core analysis presented in Talbot and Johannessen 1992, the TOC $\delta^{13}C$ in this study found greater isotopic variability in mid-Holocene sediments.

Further uncertainty in this project can be seen in the lack of sensitivity for the sugar isomer galactosan. In investigating the other isomers and their extraction efficiency compared to SRMs, galactosan had a ~200% difference from the certificate of analysis, whereas the other isomers had 60% to 90% difference. Furthermore, due to such a minimal galactosan contribution to the total sum of sugar, its relative proportion to other isomers was skewed. The ratio of mannosan/galactosan which has historically been used to delineate biomass combustion sources was unreliable due to the low concentrations of galactosan found in samples.

The elevated pyrogenic organic matter in Bosumtwi sediments has proved invaluable in assessing the fire activity and vegetative shift seen in northern Africa during the Holocene. Additional research can be done in this region on the abundances of pyrogenic matter during modern periods of climate change such as the Medieval Climate Anomaly (~1-0.8 ka) and the Little Ice Age (~0.65-0.2 ka). This study does not attempt to interpret proxies during these periods due to the lack of sample resolution in modern sediments. Given the scarcity of organic fire markers from the interior of northern Africa, further efforts should be considered to elucidate comprehensive fire reconstructions and aridity shifts associated with the end of the AHP. The ITCZ's migration southward after 5 ka contributed to a weakening monsoon, reduced vegetation, and heightened wildfire occurrence. The alignment of fire proxy peaks with recorded droughts suggests that biomass burning was a significant feedback mechanism affecting regional aridity. These findings reinforce previous studies linking fire activity, vegetation shifts, and AHP termination.

References

Abebe N. 2010. Paleohydrology of west Africa using carbonate, detrital and diagenetic minerals of lake Bosumtwi, Ghana [dissertation].[Ohio (OH)]: University of Akron

Bhattacharyya, L., Pappa, H., Russo, K. A., Sheinin, E., Williams, R. L., & Pharmacopeia, U. S. (2005). *The use of Relative Response Factors to determine impurities*. https://www.researchgate.net/publication/295423011

Bird, Michael & Wynn, Jonathan & Saiz, Gustavo & Wurster, Christopher & Mcbeath, Anna. (2014). The Pyrogenic Carbon Cycle. Annual Review of Earth and Planetary Sciences. 43. 150223150959000. 10.1146/annurev-earth-060614-105038.

Blome, M. W., Cohen, A. S., Tryon, C. A., Brooks, A. S., & Russell, J. (2012). The environmental context for the origins of modern human diversity: A synthesis of regional variability in African climate 150,000-30,000 years ago. Journal of Human Evolution, 62(5), 563–592. https://doi.org/10.1016/j.jhevol.2012.01.011

Bringué, M., Thunell, R. C., Pospelova, V., Pinckney, J. L., Romero, O. E., & Tappa, E. J. (2018). Physico-chemical and biological factors influencing dinoflagellate cyst production in the Cariaco Basin. *Biogeosciences*, *15*(8), 2325–2348. https://doi.org/10.5194/bg-15-2325-2018

Bristow, Charles & Drake, Nick & Armitage, Simon. (2009). Deflation in the dustiest place on Earth: The Bodélé Depression, Chad. Geomorphology. 105. 50-58. 10.1016/j.geomorph.2007.12.014.

Castañeda, I. S., Schouten, S., Pätzold, J., Lucassen, F., Kysemann, S., Kuhlmann, H., & Schefuß, E. (2016). Hydroclimate variability in the Nile River Basin during the past 28,000 years. *Earth and Planetary Science Letters*, *438*, 47–56. https://doi.org/10.1016/j.epsl.2015.12.014

Costa, K., Russell, J., Konecky, B.,; Lamb, H. (2014). Isotopic reconstruction of the African Humid Period and Congo Air Boundary migration at Lake Tana, Ethiopia. Quaternary Science Reviews 58–67. https://doi.org/10.1016/j.quascirev.2013.10.031

Demenocal, P., Ortiz, J., Guilderson, T., Adkins, J., Sarnthein, M., Baker, L., & Yarusinsky, M. (2000). Abrupt onset and termination of the African Humid Period: Rapid climate responses to gradual insolation forcing. *Quaternary Science Reviews*, *19*(1–5), 347–361. https://doi.org/10.1016/S0277-3791(99)00081-5

Elmquist, M., Cornelissen, G., Kukulsky, Z., and Gustafsson, O., 2006, Distinct oxidative stabilities of char versus soot black carbon: Implications for quantification and environmental recalcitrance: Global Biogeochemical Cycles, v. 20, no. 2, p. GB2009, doi: 10.1029/2005GB002629

Gasse, F. (2000). Hydrological changes in the African tropics since the Last Glacial Maximum. *Quaternary Science Reviews, 19*, 189-211.

Gosling, W. D., Miller, C. S., Shanahan, T. M., Holden, P. B., Overpeck, J. T., & van Langevelde, F. (2022). A stronger role for long-term moisture change than for CO2 in determining tropical woody vegetation change. *Science*, *376*(6593). https://doi.org/10.1126/science.abg4618

Goyal, R., sen Gupta, A., Jucker, M., & England, M. H. (2021). Historical and Projected Changes in the Southern Hemisphere Surface Westerlies. *Geophysical Research Letters*, *48*(4). https://doi.org/10.1029/2020GL090849

Hammes, K., Schmidt, M. W. I., Smernik, R. J., Currie, L. A., Ball, W. P., Nguyen, T. H., Louchouarn, P., Houel, S., Gustafsson, Ö., Elmquist, M., Cornelissen, G., Skjemstad, J. O., Masiello, C. A., Song, J., Peng, P., Mitra, S., Dunn, J. C., Hatcher, P. G., Hockyday, W. C., … Ding, L. (2007). Comparison of quantification methods to measure fire-derived (black-elemental) carbon in soils and sediments using reference materials from soil, water, sediment, and the atmosphere. Global Biogeochemical Cycles, 21(3) https://doi.org/10.1029/2006GB002914

Haug, G.H., Hughen, K.A., Sigman, D.M., Peterson, L.C., & Röhl, U. (2001). southward Migration of the Intertropical Convergence Zone Through the Holocene. *Science, 293*, 1304 - 1308

Höpker, S. N., Wu, H. C., Müller, P., Barusseau, J. P., Vernet, R., Lucassen, F., Kysemann, S. A., westphal, H. (2019). Pronounced West African Monsoon Discharge During the Mid- to Late Holocene. Frontiers in Earth Sciencehttps://doi.org/10.3389/feart.2019.00314
https://www.archaeology.wiki/blog/2017/03/23/graffiti-scribbled-ancient-cave-paintings-chad/

Hodell, D., Curtis, J., Jones, G (1991). Reconstruction of Caribbean climate change over the past 10,500 years. *Nature* **352**, 790–793 https://doi.org/10.1038/352790a0

Hodell, D., Curtis, J. & Brenner, M. (1995). Possible role of climate in the collapse of Classic Maya civilization. *Nature* **375**, 391–394 https://doi.org/10.1038/375391a0

Hubau W, Van den Bulcke J, Van Acker J, Beeckman H. Charcoal-inferred Holocene fire and vegetation history linked to drought periods in the Democratic Republic of Congo. Global Change Biology. 2015 Jun;21(6):2296-2308. DOI: 10.1111/gcb.12844. PMID: 25594742.

Jones W. B., Bacon M., Hasting D.A., 1981. The Lake Bosumtwi impact crater, Ghana. *GSA Bulletin* 1981; 92 (6): 342–349. doi: https://doi.org/10.1130/0016-7606(1981)92<342:TLBICG>2.0.CO;2

Krishnamurti, T. N. (Tiruvalam Natarajan), 1932- & Chang, C.-P. (Chih-Pei). (1987). Monsoon meteorology / edited by C.-P. Chang, T.N. Krishnamurti. New York : Oxford [Oxfordshire] : Oxford University Press ; Clarendon Press http://www.loc.gov/catdir/enhancements/fy0638/86018107-t.html

Koeberl, C., Peck, J., King, J., Milkereit, B., Overpeck, J., & Scholz, C. (2005). The ICDP Lake Bosumtwi Drilling Project: A First Report. Scientific Drilling, 1, 23–27. https://doi.org/10.2204/iodp.sd.1.04.2005

Koeberl, C., Milkereit, B., Overpeck, J. T., Scholz, C. A., Amoako, P. Y. O., Boamah, D., Danuor, S. K., Kyrp, T., Kueck, J., Hecky, R. E., King, J. W., & Peack, J. A. (2007). An international and multidisciplinary drilling project into a young complex impact structure: The 2004 ICDP Bosumtwi Crater Drilling Project - An overview. In Meteoritics and Planetary Science (Vol. 42, Issues 4–5, pp. 483–511). University of Arkansas. https://doi.org/10.1111/j.1945-5100.2007.tb01057.

Kopec, B. G., Feng, X., Posmentier, E. S., Chipman, J. W., & Virginia, R. A. (2018). Use of principal component analysis to extract environmental information from lake water isotopic compositions. *Limnology and Oceanography*, *63*(3), 1340–1354. https://doi.org/10.1002/lno.10776

Kuo, L. J., Herbert, B. E., & Louchouarn, P. (2008). Can levoglucosan be used to characterize and quantify char/charcoal black carbon in environmental media? *Organic Geochemistry*, *39*(10), 1466–1478. https://doi.org/10.1016/j.orggeochem.2008.04.026

Kröpelin, S., 2007a. High-resolution climate archives in the Sahara (Ounianga, Chad). In: Bubenzer, O., Bolten, A., Darius, F. (Eds.), Atlas of Cultural and Environmental Change in Arid Africa. Africa Praehistorica, vol. 21, pp. 56–57

Kröpelin, S., Verschuren, D., Lézine, A.-M., Eggermont, H., Cocquyt, C., Francus, P., Cazet, J.-P., Fagot, M., Rumes, B., Russell, J. M., Darius, F., Conley, D. J., Schuster, M., von Suchodoletz, H., & Engstrom, D. R. (n.d.). *Climate-Driven Ecosystem Succession in the Sahara: The Past 6000 Years*. https://www.science.org

Kuper, R., & Krö, S. (2006.). *Climate-Controlled Holocene Occupation in the Sahara: Motor of Africa's Evolution*. https://www.science.org

Leroy, S. (1995). Steps Toward Drier Climatic Conditions in northwestern Africa During the Upper Pliocene. Vrba Et Al.

Lee, C., & Olson, B. L. (1984). Dissolved, exchangeable and bound aliphatic amines in marine sediments: initial results. In *Org, Geochem* (Vol. 6).

Liu, X., Rendle-Bühring, R., Kuhlmann, H., & Li, A. (2017). Two phases of the Holocene east African Humid Period: Inferred from a high-resolution geochemical record off Tanzania. *Earth and Planetary Science Letters*, *460*, 123–134. https://doi.org/10.1016/j.epsl.2016.12.016

Louchouarn, P., Kuo, L. J., Wade, T. L., & Schantz, M. (2009). Determination of levoglucosan and its isomers in size fractions of aerosol standard reference materials. *Atmospheric Environment*, *43*(35), 5630–5636. https://doi.org/10.1016/j.atmosenv.2009.07.040

M.R. Talbot, G. Delibrias, A new late Pleistocene-Holocene water-level curve for Lake Bosumtwi, Ghana, Earth and Planetary Science Letters, Volume 47, Issue 3, 1980, Pages 336-344, ISSN 0012-821X, https://doi.org/10.1016/0012-821X(80)90020-5.

Magdi M. Ali, Radwan G. Abd Ellah, Chapter 1 - History and formation of African Lakes, Editor(s): Mostafa El-Sheekh, Hosam Easa Elsaied, Lakes of Africa, Elsevier, 2023, Pages 1-31, ISBN 9780323955270, https://doi.org/10.1016/B978-0-323-95527-0.00015-4.

Maley, J. The African rain forest vegetation and palaeoenvironments during late quaternary. Climatic Change 19, 79–98 (1991). https://doi.org/10.1007/BF00142216

Masiello, C.A., Druffel, E.R.M., and Currie, L.A., 2002, Radiocarbon measurements of black carbon in aerosols and ocean sediments: Geochimica et Cosmochimica Acta, v. 66, no. 6, p. 1025–1036, doi: 10.1016/S0016-7037(01)00831-6

Mayewski, P. A., Rohling, E. E., Stager, J. C., Kyrlén, W., Maasch, K. A., Meeker, L. D., Meyerson, E. A., Gasse, F., van Kreveld, S., Holmgren, K., Lee-Thorp, J., Rosqvist, G., Rack, F., Staubwasser, M., Schneider, R. R., & Steig, E. J. (2004). Holocene climate variability. Quaternary Research, 62(3), 243–255. https://doi.org/10.1016/j.yqres.2004.07.001

McGee, D., & deMenocal, P. B. (2017). Climatic Changes and Cultural Responses During the African Humid Period Recorded in Multi-Proxy Data. In Oxford Research Encyclopedia of Climate Science. Oxford University Press. https://doi.org/10.1093/acrefore/9780190228620.013.529

Michael R. Talbot, Truls Johannessen, A high resolution palaeoclimatic record for the last 27,500 years in tropical west Africa from the carbon and nitrogen isotopic composition of lacustrine organic matter, Earth and Planetary Science Letters, Volume 110, Issues 1–4, 1992, Pages 23-37 https://doi.org/10.1016/0012-821X(92)90036-U.

Midant-Reynes, & Beatrix. (2014). UCLA UCLA Encyclopedia of Egyptology Title Prehistoric Regional Cultures Permalink Author Publication Date Copyright Information. In *UCLA Encyclopedia of Egyptology* (Issue 1). https://escholarship.org/uc/item/4zz9t461

Mitra, S., Zimmerman, A. R., Hunsinger, G. B., Willard, D., & Dunn, J. C. (2009). A Holocene record of climate-driven shifts in coastal carbon sequestration. Geophysical Research Letters, 36(5). https://doi.org/10.1029/2008GL036875

Minnehan J. 2014. Using Sediment organic geochemistry to interpret late Holocene Barrier Island and Estuary Evolution, north Carolina, USA. [dissertation]. [North Carolina (NC)]: east Carolina University

Mertens, K. N., González, C., Delusina, I., & Louwye, S. (2009). 30 000 years of productivity and salinity variations in the late Quaternary Cariaco Basin revealed by dinoflagellate cysts. *Boreas*, *38*(4), 647–662. https://doi.org/10.1111/j.1502-3885.2009.00095.x

Moore, H. R., Crocker, A. J., Belcher, C. M., Meckler, A. N., Osborne, C. P., Beerling, D. J., & Wilson, P. A. (2022). Hydroclimate variability was the main control on fire activity in northern Africa over the last 50,000 years. *Quaternary Science Reviews*, *288*. https://doi.org/10.1016/j.quascirev.2022.107578

Nicholson, S. E. (1981). Rainfall and Atmospheric Circulation during Drought Periods and Wetter Years in West Africa. *Monthly Weather Review*, *109*(10), 2191-2208. https://doi.org/10.1175/1520-0493(1981)109<2191:RAACDD>2.0.CO;2
Nicholson, S. E. (2018). The ITCZ and the seasonal cycle over equatorial Africa. *Bulletin of the American Meteorological Society*, *99*(2), 337–348. https://doi.org/10.1175/BAMS-D-16-0287.1

Niedermeyer, E. M., Schefuß, E., Sessions, A. L., Mulitza, S., Mollenhauer, G., Schulz, M., & Wefer, G. (2010). Orbital- and millennial-scale changes in the hydrologic cycle and vegetation in the western African Sahel: Insights from individual plant wax δD and δ13C. *Quaternary Science Reviews*, *29*(23–24), 2996–3005. https://doi.org/10.1016/j.quascirev.2010.06.039

Otu M. 2010. The origin, transformation, and deposition of sediments in Lake Bosomtwe/Bosumtwi (Ghana, west Africa) [dissertation]. [Ontario, Canada (ON)]: University of Waterloo

Patel, N. 2011. Holocene Climate and Carbon Sequestration via Black Carbon Burial in Sediments. [Thesis]. [North Carolina (NC)]: east Carolina University

Pattnayak, K. C., Abdel-Lathif, A. Y., Rathakrishnan, K. v., Singh, M., Dash, R., & Maharana, P. (2019). Changing Climate Over Chad: Is the Rainfall Over the Major Cities Recovering? *Earth and Space Science*, *6*(7), 1149–1160. https://doi.org/10.1029/2019EA000619

Pausata, F. S. R., Gaetani, M., Messori, G., Berg, A., Maia de Souza, D., Sage, R. F., & deMenocal, P. B. (2020). The Greening of the Sahara: Past Changes and Future Implications. In *One Earth* (Vol. 2, Issue 3, pp. 235–250). Cell Press. https://doi.org/10.1016/j.oneear.2020.03.002

Peck, J. A., Green, R. R., Shanahan, T., King, J. W., Overpeck, J. T., & Scholz, C. A. (2004). A magnetic mineral record of Late Quaternary tropical climate variability from Lake Bosumtwi, Ghana. *Palaeogeography, Palaeoclimatology, Palaeoecology*, *215*(1–2), 37–57. https://doi.org/10.1016/S0031-0182(04)00438-9

Pedersen, J. (1995). Drought, Migration and Population Growth in the Sahel: The Case of the Malian Gourma: 1900-1991. In *Studies* (Vol. 49, Issue 1).

Peterson, L. C., Murray, R. W., King, J. W., Peterson, L., Haug, G., Murray, R., Yarincik, K., King, J., Bralower, T., Kymeo, K., Rutherford, S., & Pearce, R. (2000). 4. LATE QUATERNARY STRATIGRAPHY AND SEDIMENTATION AT SITE 1002, CARIACO BASIN (VENEZUELA) 1. In *Scientific Results* (Vol. 165). https://www.researchgate.net/publication/228807994

Poot, A., Quik, J. T. K., Veld, H., & Koelmans, A. A. (2009). Quantification methods of Black Carbon: Comparison of Rock-Eval analysis with traditional methods. In *Journal of Chromatography A* (Vol. 1216, Issue 3, pp. 613–622). https://doi.org/10.1016/j.chroma.2008.08.011

Poyrazli, H. 2010. Reconstruction of Lake-Level Variation and Shoreline Position of Lake Bosumtwi, Ghana for the Last 0.5 Ma [thesis]. [Ohio (OH)]: University of Akron

Prasetyo, E., Jatmiko, T. H., & Kyrimy, M. F. (2019). Optimization Study of Charcoal Observation with Scanning Electron Microscope in Various Operating Conditions. IOP Conference Series: Earth and Environmental Science, 251(1). https://doi.org/10.1088/1755-1315/251/1/012010

Prell, W.L., Murray, D.W., Clemens, S.C. and Anderson, D.M. (1992). Evolution and Variability of the Indian Ocean Summer Monsoon: Evidence from the Western Arabian Sea Drilling Program. In Synthesis of Results from Scientific Drilling in the Indian Ocean (eds R.A. Duncan, D.K. Rea, R.B. Kidd, U. von Rad and J.K. Weissel). https://doi.org/10.1029/GM070p0447

Rohling, E. J., Marino, G., & Grant, K. M. (2015). Mediterranean climate and oceanography, and the periodic development of anoxic events (sapropels). In *Earth-Science Reviews* (Vol. 143, pp. 62–97). Elsevier B.V. https://doi.org/10.1016/j.earscirev.2015.01.008

Russell, J., Talbot, M., & Haskell, B. (2003). Mid-holocene climate change in Lake Bosumtwi, Ghana. Quaternary Research, 60(2), 133-141. doi:10.1016/S0033-5894(03)00065-6

Schummer, C., Delhomme, O., Appenzeller, B. M. R., Wennig, R., & Millet, M. (2009). Comparison of MTBSTFA and BSTFA in derivatization reactions of polar compounds prior to GC/MS analysis. *Talanta*, *77*(4), 1473–1482. https://doi.org/10.1016/j.talanta.2008.09.043

Sha, L., Ait Brahim, Y., Wassenburg, J. A., Yin, J., Peros, M., Cruz, F. W., Cai, Y., Li, H., Du, W., Zhang, H., Edwards, R. L., & Cheng, H. (2019). How Far north did the African Monsoon Fringe Expand During the African Humid Period? Insights From southwest Moroccan Speleothems. *Geophysical Research Letters*, *46*(23), 14093–14102. https://doi.org/10.1029/2019GL084879

Shanahan, T. M. (2006). west african monsoon variability from a high-resolution paleolimnological record (lake bosumtwi, Ghana [dissertation]. [Akynsas (AZ)]: University of Arizona

Shanahan, T. M., Mckyy, N. P., Hughen, K. A., Overpeck, J. T., Otto-Bliesner, B., Heil, C. W., King, J., Scholz, C. A., & Peck, J. (2015). The time-transgressive termination of the African humid period. 2015 Nature Geoscience, 8(2), 140–144. https://doi.org/10.1038/ngeo2329

Shanahan, T. M., Overpeck, J. T., Wheeler, C. W., Beck, J. W., Pigati, J. S., Talbot, M. R., Scholz, C. A., Peck, J., & King, J. W. (2006). Paleoclimatic variations in west Africa from a record of late Pleistocene and Holocene Lake level stands of Lake Bosumtwi, Ghana. Palaeogeography, Palaeoclimatology, Palaeoecology, 242(3–4), 287–302. https://doi.org/10.1016/j.palaeo.2006.06.007

Shanahan, T. M., Overpeck, J. T., Beck, J. W., Wheeler, C. W., Peck, J. A., King, J. W., & Scholz, C. A. (2008). The formation of biogeochemical laminations in Lake Bosumtwi, Ghana, and their usefulness as indicators of past environmental changes. *Journal of Paleolimnology*, *40*(1), 339–355. https://doi.org/10.1007/s10933-007-9164-4

Shanahan, T. M., Beck, J. W., Overpeck, J. T., McKyy, N. P., Pigati, J. S., Peck, J. A., Scholz, C. A., Heil, C. W., & King, J. (2012). Late Quaternary sedimentological and climate changes at Lake Bosumtwi Ghana: New constraints from laminae analysis and radiocarbon age modeling. *Palaeogeography, Palaeoclimatology, Palaeoecology*, *361–362*, 49–60. https://doi.org/10.1016/j.palaeo.2012.08.001

Shanahan, T. M., Peck, J. A., McKyy, N., Heil, C. W., King, J., Forman, S. L., Hoffmann, D. L., Richards, D. A., Overpeck, J. T., & Scholz, C. (2013). Age models for long lacustrine sediment records using multiple dating approaches - An example from Lake Bosumtwi, Ghana. *Quaternary Geochronology*, *15*, 47–60. https://doi.org/10.1016/j.quageo.2012.12.001

Shanahan, T., Hughen, K., McKyy, N. et al.,. CO2 and fire influence tropical ecosystem stability in response to climate change. Sci Rep 6, 29587 (2016). https://doi.org/10.1038/srep295872001

Slowik, J. G., Cross, E. S., Han, J. H., Davidovits, P., Onasch, T. B., Jayne, J. T., Williams, L. R., Canagaratna, M. R., Worsnop, D. R., Chakrabarty, R. K., Moosmüller, H., Arnott, W. P., Schwarz, J. P., Gao, R. S., Fahey, D. W., Kok, G. L., & Petzold, A. (2007). An Inter-Comparison of Instruments Measuring Black Carbon Content of Soot Particles. Aerosol Science and Technology, 41(3), 295–314. https://doi.org/10.1080/02786820701197078.

Stevens, H., Barmuta, L. A., Chase, Z., Saunders, K. M., Zawadzki, A., Bowie, A. R., Perron, M. M. G., Sanz Rodriguez, E., Paull, B., Child, D. P., Hotchkis, M. A. C., & Proemse, B. C. (2024). Comparing levoglucosan and mannosan ratios in sediments and corresponding aerosols from recent Australian fires. *Science of the Total Environment*, *945*. https://doi.org/10.1016/j.scitotenv.2024.174068

Sutcliffe, J. v., Dugdale, G., & Milford, J. R. (1989). The sudan floods of 1988. *Hydrological Sciences Journal*, *34*(3), 355–364. https://doi.org/10.1080/02626668909491339

Taiz, L., Zeiger, E., Møller, I. M., & Murphy, A. (2015). Plant physiology and development (6th ed.). Sinauer Associates.

Talbot, M. R., Livingstone, D. A., Palmer, C., Maley, J., Melack, J. M., Delibrias, G., & Gulliksen, S. (1984). Preliminary results from sediment cores from Lake Bosumtwi, Ghana. *Palaeoecology of Africa and the Surrounding Islands*, 16, 173–192.

Tan, Z., Yuan, Y., Gu, M., Han, Y., Mao, L., Tan, T., Wu, C.; Han, T. (2023). Levoglucosan and its isomers in terrestrial sediment as a molecular markers provide direct evidence for the low-temperature fire during the mid-Holocene in the northern Shandong Peninsula of China. Quaternary International. https://doi.org/10.1016/j.quaint.2023.05.010

Thevenon, F., Williamson, D., Bard, E., Anselmetti, F. S., Beaufort, L., & Cachier, H. (2010). Combining charcoal and elemental black carbon analysis in sedimentary archives: Implications for past fire regimes, the pyrogenic carbon cycle, and the human-climate interactions. *Global and Planetary Change*, *72*(4), 381–389. https://doi.org/10.1016/j.gloplacha.2010.01.014

Tuenter, E., Weber, S.L., Hilgen, F.J., Lourens, L.J., 2003. The response of the African summer monsoon to remote and local forcing due to precession and obliquity. Glob. Planet. Chang. 36, 219e235. https://doi.org/10.1016/S0921-8181(02) 00196-0

Trentin, F. A., Cagliari, J., Kochhann, K. G. D., & Frank, T. (2025). Chemical weathering proxies: An assessment of their robustness to reconstruct Paleozoic climate conditions. *Evolving Earth*, *3*, 100054. https://doi.org/10.1016/j.eve.2024.100054

van der Meeren, T., Verschuren, D., Sylvestre, F., Nassour, Y. A., Naudts, E. L., Aguilar Ortiz, L. E., Deschamps, P., Tachikywa, K., Bard, E., Schuster, M., & Abderamane, M. (2022). Van der Meeren et al A predominantly tropical influence on late Holocene hydroclimate variation in the hyperarid central Sahara. In *Sci. Adv* (Vol. 8). https://www.science.org

Vallé, F., Dupont, L. M., Leroy, S. A. G., Schefuß, E., & Wefer, G. (2014). Pliocene environmental change in west Africa and the onset of strong NE trade winds (ODP Sites 659 and

658). *Palaeogeography, Palaeoclimatology, Palaeoecology*, *414*, 403–414. https://doi.org/10.1016/j.palaeo.2014.09.023
Vinnepand, M., Zeeden, C……2024. Quaternary Science Reviews 325….

Wright, D. K. (2017). Humans as agents in the termination of the African humid period. *Frontiers in Earth Science*, *5*. https://doi.org/10.3389/feart.2017.00004

Weldeab, S., Schneider, R. R., Kölling, M., & Wefer, G. (2005). Holocene African droughts relate to eastern equatorial Atlantic cooling. Geology, 33(12), 981–984. https://doi.org/10.1130/G21874.1

APPENDIX – Background, Methodological Details and Interpretations

Appendix – Supplementary Figures

Appendix - Supplementary Table

Background

Differences between individual cores taken from the middle of lake Bosumtwi can be seen in Appendix Figure 1, proxies such as magnetic susceptibility allows for downcore correlation between different cores. In 5C, the depth intervals of interest (>3.4m) and the positioning of the sapropel layer is close in depth to that of 5B and 3P. Distinct differences between these cores could lie in the compaction and post-depositional alterations such as diageneses (Shanahan et al,, 2012).

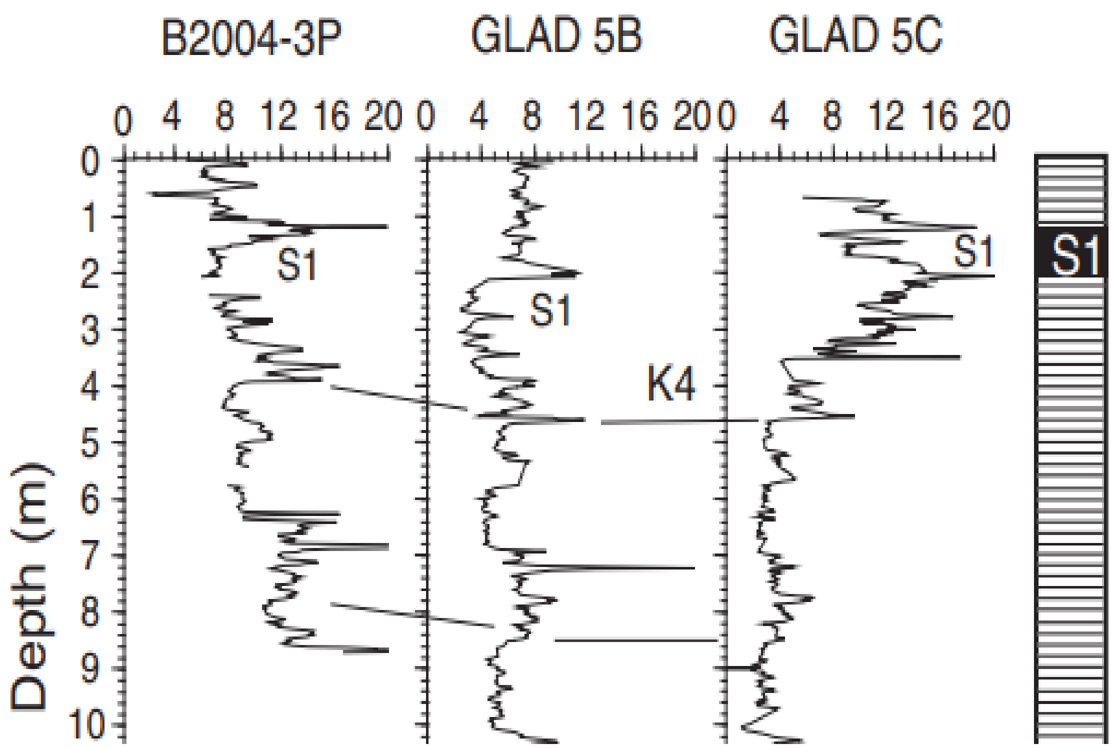

Appendix Figure 1. Age correlation across cores in Lake Bosumtwi, using Magnetic Susceptibility (10^{-5} SI units) in cores 3P, 5B and 5C (Shanahan et al 2012).

Methodology Details

GCMS QP-2010S Calibration, Method and Retention times

The retention times for levoglucosan and its isomers were determined before sample analysis by injection of pure standards and verified through the extraction of SRMs (Standard Reference Material). The identification of these compounds was done via mass to charge ratio (m/z) as well as specific mass fragmentation patterns (qualifier ions) of each isomer. The injection mode for the GC component was set to splitless at a temperature of 270°C. The column oven temperature was programmed to reach 65°C and held for 2 minutes before ramping up to 250°C and held for 5 minutes at a rate of 4°C per minute. The ion source temperature in the MS component was set to 200°C with an interface temperature of 310°C. The GCMS method was set to SIM (Select Ion Monitoring) to filter out compounds outside of our specified windows for detection.

Table 1. Retention window for standards and their associated qualifier ions

Standard	Retention time(min)	Mass/Charge ratio(m/z)	Secondary ion 1	Ion 2	Ion 3	Ion 4	Ion 5
Levoglucosan (1,6-Anhydro-β-D-glucose)	27.95	204.1	217.1	147.1	129.1	75.05	333.2
Galactosan (1,6-Anhydro-D-galactose)	26.65	220.15	206.1	221.1	147.1	75	74.05
Mannosan (1,6-anhydro-β-D-mannopyranose)	27.3	217.15	204.15	147.1	129.1	75.05	74.05
C^{13} Labelled Levoglucosan (1,6-Anhydro-β-D-glucose (levoglucosan) (U-$^{13}C_6$, 98%))	27.85	206.1	220.1	75.1	147.1	74.1	132

Minimum Detectable Quantity of elemental and sugar analysis

MDQ for C_{Soot} from the Light Stable Isotope Mass Spectrometry Laboratory in the Department of Geological Sciences at the University of Florida requires ~20µg of BC in samples. The MDQ for levoglucosan and its isomers was established through serial dilutions of pure standards provided by the Cambridge Isotope Lab. The dilutions were injected into the GCMS at known concentrations until a signal to noise ratio (S/N) of ~8-3 was reached. A S/N ratio in that window is used to determine the minimum quantifiable amount.

Relative Response Factor (RRF)

RRF is an analytic measurement used in chromatography analysis as a form of QAQC (Quality Assurance and Quality Control) when samples are being extracted and injected into an instrument. For each batch of levoglucosan samples derivatized, an RRF was derivatized and injected as well. The RRF was made up of known concentrations of standards and was useful in gauging the efficiency of not only the derivatization in actual samples but also the instrument, as impurities can dampen analytic responses (Bhattacharyya et al 2005). After samples and RRFs are injected into the GCMS, the responses of each analyte are normalized based on the relative response of the internal standard (C^{13} labeled levoglucosan) in each sample.

Derivatization

Derivatization is the process of chemically altering an analyte to improve chromatograph analytics (Schummer et al 2009). The purpose of using BSTFA [bis (trimethylsilyl) trifluoroacetamide] as a derivatizing agent is to replace polar functional groups such as OH-groups with a nonpolar trimethylsilyl (TMS) functional group. This is necessary to improve the quality analysis on a GCMS.

Interpretations

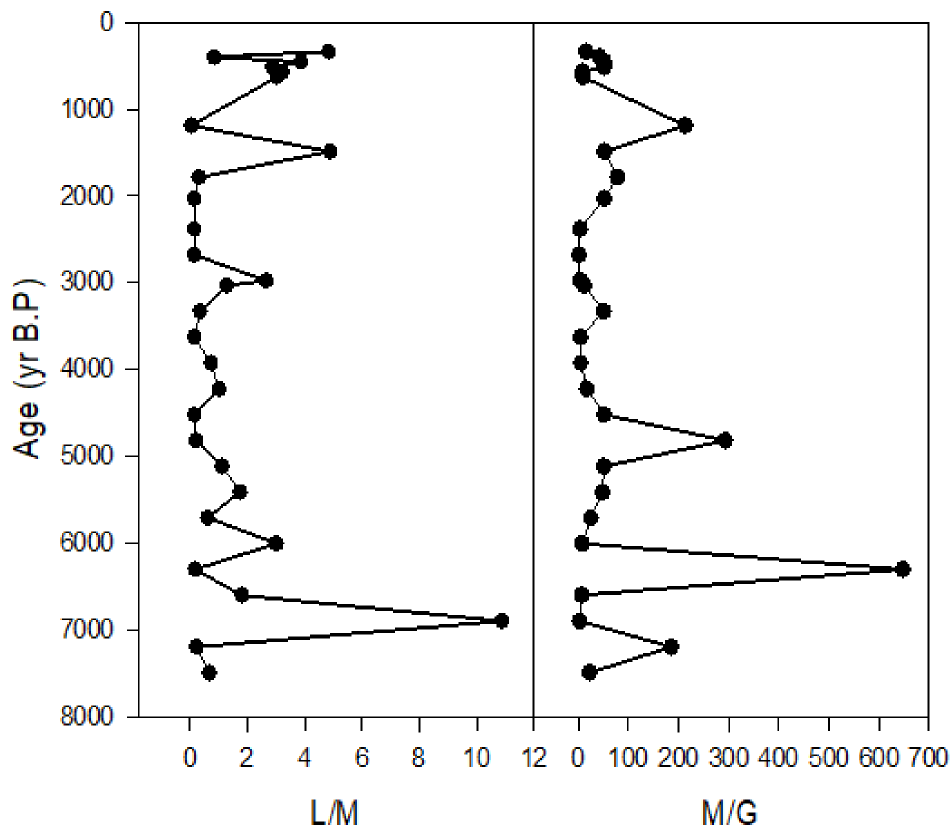

Appendix Figure 2. Ratio of the concentrations of Levoglucosan to Mannosan (left) and Mannosan to Galactosan (right) from BOS04-5C.

L/M and M/G

The levoglucosan to mannosan abundance had an average ratio of 1.75, the maximum occurs at 6.9 ka with a ratio of 10.86. At the end of the AHP the L/M average was 2.24, after the peak seen at 6.9 ka the ratio decreases until 5 ka with an average of 1.4 during this period.

Post-AHP, a decrease in relative sugar concentrations was seen between 5 ka and 3.2 ka averaging at 0.42. After 3 ka, there were 3 periods of relative increase in sugar concentration observed at 3 ka to 2.9 ka, 1.4 ka, and between 0.6 ka to 0.3 ka with averaged values of 1.96, 4.88 and 3.10.

The ratio of mannosan to galactosan averaged 68.95 with the maximum value of 647 occurring at 6.3 ka. Between 7.4 ka and 5 ka the average was 110.4. After the end of the AHP (5 ka to 0.3 ka) the average was 50.29. There are 4 distinct periods of elevated M/G at 7.2 ka, 6.3 ka, 4.8 ka and at 1.1 ka, with values of 185, 647, 292, 213, respectively.

The proportional ratio of the isomers is due to the biomass source of combustion as well as the relative degradation rates of isomers. Levoglucosan has a higher rate of degradation than mannosan in lake sediments, hindering the proxy's ability to accurately discriminate biomass sources (Stevens et al.,2024). The ratio of L/M (Appendix Fig. 2) has historically been used to discriminate the source of low temperature biomass combustion (Tan et al.,2023), typically in conjunction with M/G. However, the low concentrations of galactosan isomer skew the M/G ratio outside of publicized ranges used for biomass sourcing. Studies have suggested that the combustion of softwoods results in levoglucosan/mannosan (L/M) and mannosan/galactosan (M/G) ratios of (0.7-7) and (0.7-8), respectively. The combustion of hardwoods yielded L/M and M/G ratios of (>7) and (>0.7), respectively. The combustion of grasses and straws produced L/M and M/G ratios of (>7) and (<0.7), respectively.

ODP & GeoB proxies

Ti% from ODP 1002

The Ti% in ODP-1002 sediments shows higher abundance between 7.5-5 ka with an overall average of 0.24% over the last 7.5 ka. During the AHP, the Ti% averaged 0.31%, compared to the 0.21% average post-AHP. Titanium is a reliable proxy for tracking precipitation changes because it is unaffected by chemical or biological mediation. Titanium is a terrestrially derived element, increases in Ti% in the sediment record reflect increased weathering, erosion, and terrestrial input as a product of increased precipitation. The titanium abundance dataset used in this study is from Haug et al. (2001 and is used to investigate the southwards shift of the ITCZ. The publication found fluctuations in Ti% that coincide with the timing of global climate shifts such as the Younger Dryas (12.9- 11.6 ka), the Holocene 'Thermal maximum'(10.5- 5.4 ka), the 'Medieval Climate Anomaly'(1- 0.8 ka), and the 'Little Ice Age' (0.65- 0.2 ka).

Charcoal from BOS05B/5C

Charcoal, unlike soot, is useful for understanding local fire activity due to its lack of aeolian transportation. The charcoal analysis was performed by sorting a minimum of 2000 charcoal fragments above 10 μm and normalized to time (particles/cm^2/yr)

δ^2D of C_{31} n-alkane in leaf wax from Lake Bosumtwi

The hydrogen isotopes datasets incorporated into this project are useful for understanding paleo-hydrological changes. The n-alkanes are long chain hydrocarbons found in waxy cuticles of terrestrial vegetation that are preserved in sedimentary records. The δD reflects the mass-dependent fractionation process of precipitation, thus needs to be corrected for global ice volume. The n-alkanes are extracted and analyzed on a GCMS; the isotope analysis was done using a Delta V isotope ratio mass spectrometer via a pyrolysis interface ran at 1430°C (Shanahan et al., 2015).

<u>PCA</u>

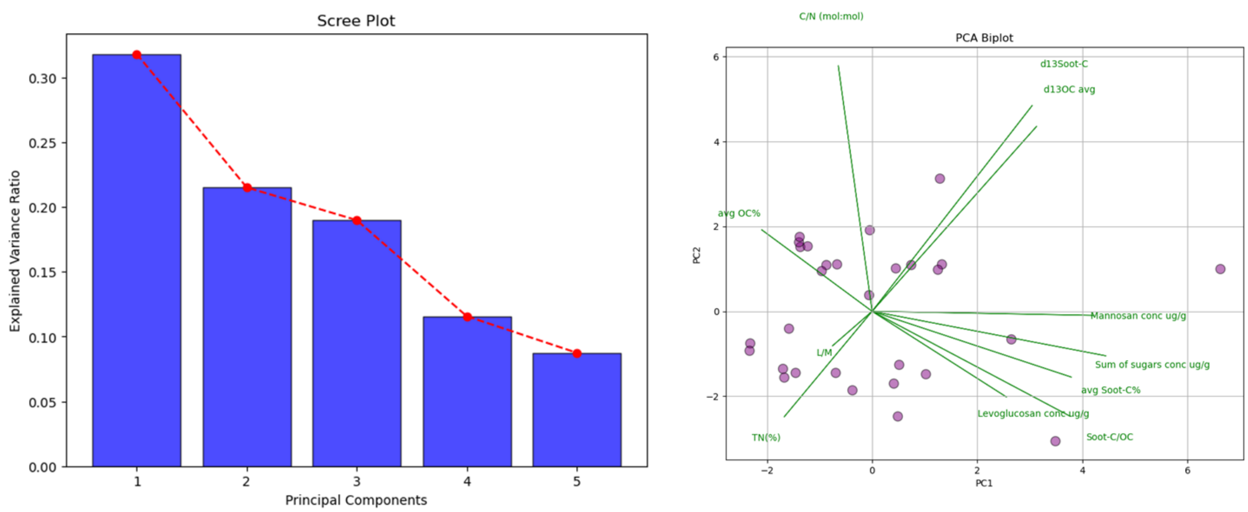

Appendix Figure 3. PCA scree plot (left) and biplot (right) made using Python, shows the relation between different proxies used in this study.

Principle Component Analysis (PCA) is a useful statistical technique for identifying underlying correlation and shows the variability data set, having been used in multiple geologic applications (Kopec et al., 2018, Trentin et al., 2024). The scree plot does not have a significant drop off between the 1st and the following principal component, meaning that there are similar amounts of variance between all the data. In the Biplot, the adjacent vectors that make a small angel are positively correlated. Opposing vectors have a negative correlation while perpendicular vectors suggest no correlation. There was a positive correlation between the isotopic ranges of soot and TOC, which was to be expected. These isotopic ranges have a negative correlation with TN% and L/M. While showing little to no correlation with the sugar concentrations, avg TOC%, avg Soot-C%, and $C_{Soot/TOC}$.

Comparing extracted Standard Reference Material (SRM) to their certification of analysis

The accuracy and precision of the levoglucosan isomer extraction was verified through the extractions of Standard Reference Materials (SRM). Both SRM 1649a and 2787 have been analyzed by Louchouarn et al and Kou et al. On average the levoglucosan and mannosan isomers had a ~85% and ~70% difference from the SRM certificate of analysis and analysis by Louchouarn et al. However, the difference in the concentrations of galactosan to the target concentrations was significantly greater than the other isomers averaging a 198% difference from the target concentrations.

Kuo et al. (2008a) and Louchouarn et al. (2009) have both analyzed SRM 1649a for levoglucosan and its isomers. These publications compared the extraction efficiency of these sugars under different extraction protocols, using different surrogate standards (isotopically labeled d7-levoglucosan vs. sedoheptulosan) and different solvents (100% ethyl acetate vs DCM: MeOH). SRM 1649a was extracted for this study using 1:1 Acetone: Hexane solvent and the same extraction method for samples. The only difference in extraction protocol lies in the use of a glass fiber filter to filter out particulate matter in the supernatant before being transferred to a rotovap flask. This extraction recorded sugar concentrations at ~30% compared to Louchouarn. However, the proportion of isomer concentrations was consistent, except for Galactosan. This difference in concentration could be due to the age and storage of the SRM. The certificate of analysis only looks at the concentration of levoglucosan 81.1 ± 6.1 (µg/g).

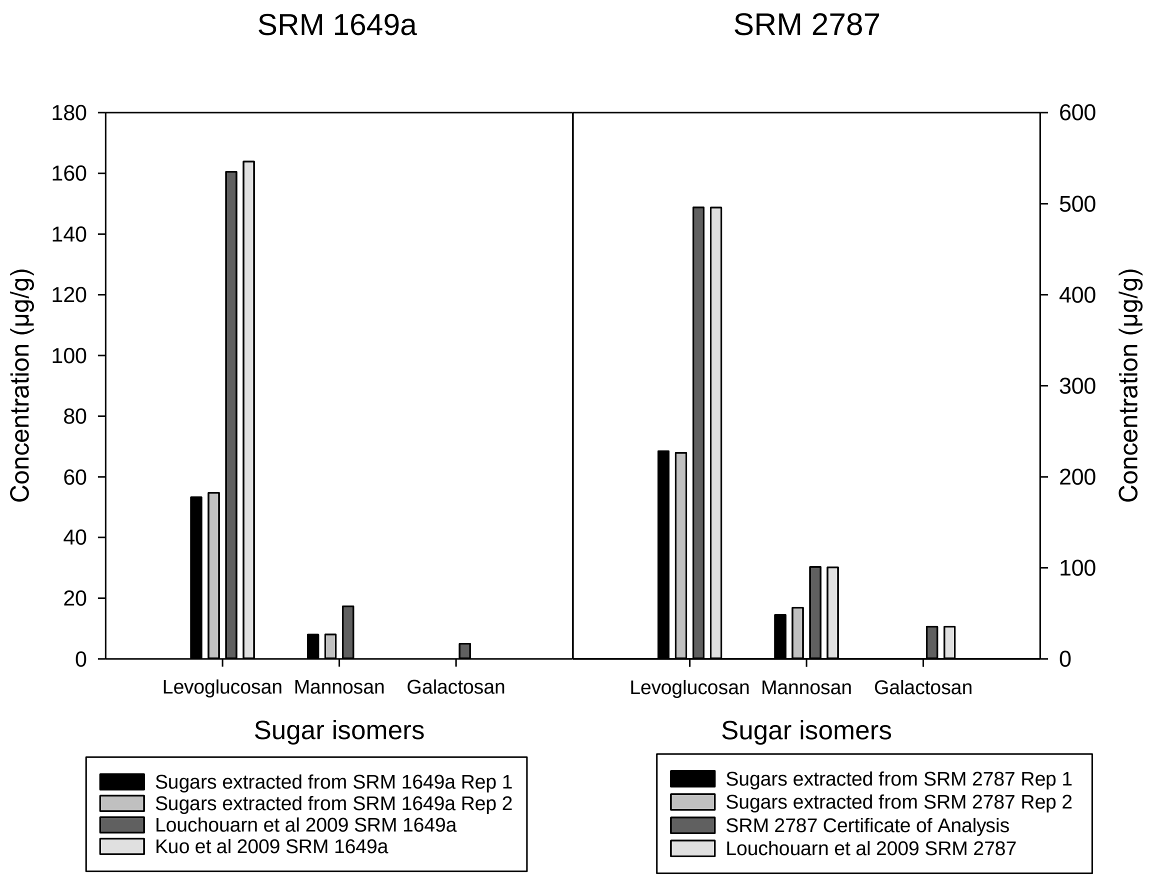

Appendix Figure 4. Comparing the levoglucosan isomer extraction efficiency against SRM 1649a, SRM 2787 and other publications (Kuo et al., 2009; Louchouarn et al., 2009)

Appendix References

Bhattacharyya, L., Pappa, H., Russo, K. A., Sheinin, E., Williams, R. L., & Pharmacopeia, U. S. (2005). *The use of Relative Response Factors to determine impurities*. https://www.researchgate.net/publication/295423011

Haug, G.H., Hughen, K.A., Sigman, D.M., Peterson, L.C., & Röhl, U. (2001). southward Migration of the Intertropical Convergence Zone Through the Holocene. *Science, 293*, 1304 – 1308.

Kopec, B. G., Feng, X., Posmentier, E. S., Chipman, J. W., & Virginia, R. A. (2018). Use of principal component analysis to extract environmental information from lake water isotopic compositions. *Limnology and Oceanography*, *63*(3), 1340–1354. https://doi.org/10.1002/lno.10776

Kuo, L. J., Herbert, B. E., & Louchouarn, P. (2008). Can levoglucosan be used to characterize and quantify char/charcoal black carbon in environmental media? *Organic Geochemistry*, *39*(10), 1466–1478. https://doi.org/10.1016/j.orggeochem.2008.04.026

Louchouarn, P., Kuo, L. J., Wade, T. L., & Schantz, M. (2009). Determination of levoglucosan and its isomers in size fractions of aerosol standard reference materials. *Atmospheric Environment*, *43*(35), 5630–5636. https://doi.org/10.1016/j.atmosenv.2009.07.040

Schummer, C., Delhomme, O., Appenzeller, B. M. R., Wennig, R., & Millet, M. (2009). Comparison of MTBSTFA and BSTFA in derivatization reactions of polar compounds prior to GC/MS analysis. *Talanta*, *77*(4), 1473–1482. https://doi.org/10.1016/j.talanta.2008.09.043

Shanahan, T. M., Beck, J. W., Overpeck, J. T., McKyy, N. P., Pigati, J. S., Peck, J. A., Scholz, C. A., Heil, C. W., & King, J. (2012). Late Quaternary sedimentological and climate changes at Lake Bosumtwi Ghana: New constraints from laminae analysis and radiocarbon age modeling. *Palaeogeography, Palaeoclimatology, Palaeoecology*, *361–362*, 49–60. https://doi.org/10.1016/j.palaeo.2012.08.001

Stevens, H., Barmuta, L. A., Chase, Z., Saunders, K. M., Zawadzki, A., Bowie, A. R., Perron, M. M. G., Sanz Rodriguez, E., Paull, B., Child, D. P., Hotchkis, M. A. C., & Proemse, B. C. (2024). Comparing levoglucosan and mannosan ratios in sediments and corresponding aerosols from recent Australian fires. *Science of the Total Environment*, *945*. https://doi.org/10.1016/j.scitotenv.2024.174068

Tan, Z., Yuan, Y., Gu, M., Han, Y., Mao, L., Tan, T., Wu, C.; Han, T. (2023). Levoglucosan and its isomers in terrestrial sediment as a molecular markers provide direct evidence for the low-temperature fire during the mid-Holocene in the northern Shandong Peninsula of China. Quaternary International. https://doi.org/10.1016/j.quaint.2023.05.010

Trentin, F. A., Cagliari, J., Kochhann, K. G. D., & Frank, T. (2025). Chemical weathering proxies: An assessment of their robustness to reconstruct Paleozoic climate conditions. *Evolving Earth*, *3*, 100054. https://doi.org/10.1016/j.eve.2024.100054